iScience

Article

Topical rewetting restores the autoimmune-damaged corneal stroma

Graphical abstract

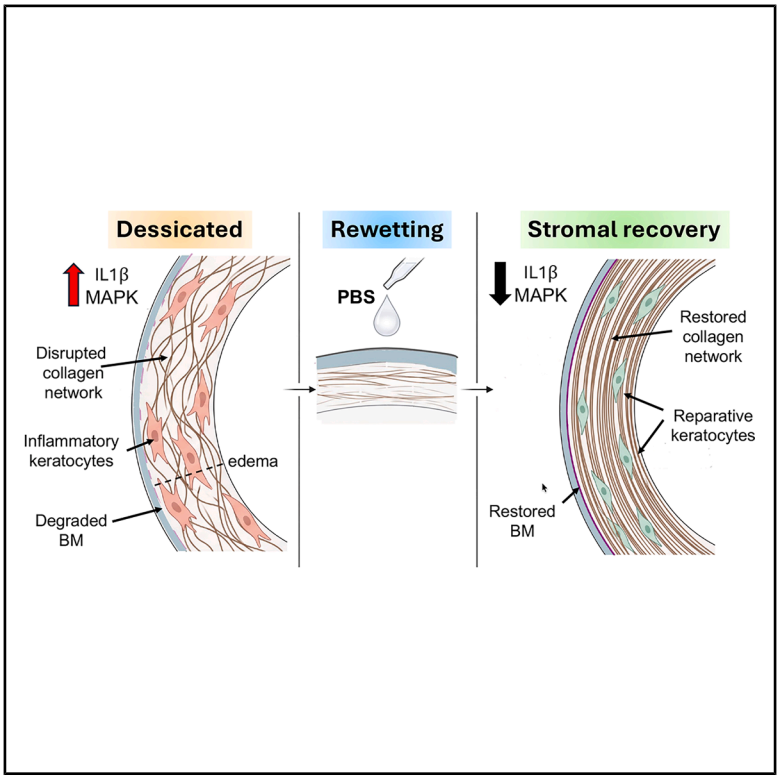

Authors

Yael Efraim, Yu Ting Chen, Luye An, ..., Hanan Sinada, Nancy A. McNamara, Sarah M. Knox

Correspondence

nmcnamara@berkeley.edu (N.A.M.), sarah.knox@ucsf.edu (S.M.K.)

In brief

Cell biology; transcriptomics

Highlights

- Aqueous deficiency disrupts corneal stromal architecture and keratocyte homeostasis
- Rewetting restores stromal collagen organization and the basement membrane
- Keratocyte plasticity underlies inflammatory-to-reparative state transition
- Rewetting dampens IL-1β-MAPK signaling, contributing to stromal restoration

Efraim et al., 2026, iScience *29*, 116130
June 19, 2026
https://doi.org/10.1016/j.isci.2026.116130

CellPress

iScience

CellPress
OPEN ACCESS

Article

Topical rewetting restores the autoimmune-damaged corneal stroma

Yael Efraim,[1,4] Yu Ting Chen,[1,4] Luye An,[1,4] Seyyed Vahid Niknezhad,[1] Dylan Pham,[1] Ka Neng Cheong,[1] Mario A. Robledo,[1] Hanan Sinada,[1] Nancy A. McNamara,[2,3,*] and Sarah M. Knox[1,5,*]

[1]Department of Cell & Tissue Biology, School of Dentistry, University of California, San Francisco, San Francisco, CA 94143, USA
[2]School of Optometry and Vision Science Graduate Program, University of California, Berkeley, Oakland, CA 94720, USA
[3]Department of Anatomy, University of California, San Francisco, San Francisco, CA 94143, USA
[4]These authors contributed equally
[5]Lead contact
*Correspondence: nmcnamara@berkeley.edu (N.A.M.), sarah.knox@ucsf.edu (S.M.K.)
https://doi.org/10.1016/j.isci.2026.116130

SUMMARY

Corneal wetting is the most common treatment for dry eye disease and is generally considered palliative. Here, we challenge this view by demonstrating that rewetting the desiccated cornea of an aqueous-deficient mouse model with the simplest rewetting agent, phosphate-buffered saline (PBS), is sufficient to restore the severely disrupted collagen-rich stromal architecture required for transparency. Using transmission electron microscopy, we show substantial recovery of stromal organization, including a marked reduction in interfibrillar spacing consistent with resolution of stromal edema, following rewetting. Single-cell transcriptomic analyses further reveal that stromal keratocytes transition from an inflammatory state to a reparative-like phenotype in response to rewetting alone, demonstrating keratocyte plasticity and the potential regenerative function of rewetting. This reparative shift is mediated, in part, by dampening of IL-1β associated MAPK signaling. Together, these findings uncover an unexpected regenerative capacity of corneal rewetting and redefine its therapeutic impact in dry eye disease.

INTRODUCTION

A healthy tear film is crucial for vision, tissue function, and protection from environmental, inflammatory, and microbial insult. Prolonged dryness, as seen in aqueous-deficient dry eye, triggers a vast array of pathological alterations in cell phenotypes and corneal structure. Despite the high prevalence of dry eye globally,[1] effective treatments are limited, with the most common therapy being over-the-counter (OTC) topical lubricants and rewetting drops.[1] As the apical epithelial layers show very little to no recovery with the routine application of OTC dry eye products in both human patients and mouse models,[2,3] saline-based solutions are generally considered non-regenerative. However, studies to date have overlooked the collagen-rich stromal compartment that is critically important for vision, serving to maintain transparency, avascularity, and refractive power, while also providing essential mechanical strength and preserving corneal shape through its highly organized structure of densely packed collagen fibrils (predominantly types 1 and 5)[4,5] arranged as lamellae parallel to the epithelial surface.[6] This robust extracellular matrix (ECM) is enriched with a diverse array of proteoglycans, including perlecan and glycoproteins, such as thrombospondin that regulate the size and organization of the fibers as well as cell-to-cell and cell-to-matrix interactions[5]

The primary cells responsible for establishing and maintaining this complex architecture are stromal keratocytes. These specialized, largely quiescent cells, derived from the neural crest, maintain the aligned collagen nanofibrils and the composition of the stroma under homeostatic conditions. Notably, single-cell sequencing studies of healthy whole cornea have revealed heterogeneity within keratocyte populations in both murine (3 subtypes) and human (4 subtypes) stroma.[7] *In vivo* confocal microscopy (IVCM) of dry eye patients, including those with the autoimmune disease Sjogren's, has demonstrated significant alterations in stromal keratocytes, showing their transition to an activated, fibroblast-like phenotype associated with corneal injury and stromal inflammation.[8–11] While murine models of acute corneal damage have shown that keratocytes undergo apoptosis or differentiate into activated fibroblasts and myofibroblasts that possess reparative functions,[12] the impact of chronic inflammatory conditions, such as aqueous-deficient dry eye, on the heterogeneity and plasticity of keratocytes, and the specific signaling pathways governing their behavior, remains unclear. Furthermore, despite their close proximity to the overlying epithelium via the basement membrane (BM), it is still unknown whether changes at the ocular surface, can trigger keratocytes to adopt disruptive or regenerative states.

Using the autoimmune-regulator knock out (*Aire* KO or KO) mouse model to mimic the pathological features of aqueous-deficient dry eye,[13] we discovered that application of preservative-free phosphate buffer saline (PBS), the simplest form of

rewetting agents, induces the generation of a heterogeneous pool of reparative keratocytes, transitioning them from inflammatory to reparative phenotype that drives stromal repair. Accordingly, PBS restored stromal architecture to a homeostatic-like state while initiating the repair of the BM, suggesting the re-establishment of matrix-cell communication. Importantly, treatment disrupted a chronically active MAPK signaling pathway, presumably stimulated by IL1, that is among the most common mediators of tissue damage but untested for its impact on the stroma. Thus, contrary to our prevailing belief that topical saline-like lubricants for dry eye disease are largely palliative, we show that PBSs application to the desiccated ocular surface effectively reinstates key aspects of keratocyte function required for stromal regeneration.

RESULTS

Intermittent rewetting of the ocular surface with PBS restores the structural integrity of the stroma

Reflex tear secretion in response to changes at the ocular surface is essential to maintain corneal homeostasis and promote wound healing, all of which are profoundly reduced with dry eye disease.[14] Topical aqueous wetting is a well-established palliative therapy for relieving symptoms of chronic dry eye[15] but has not been shown to restore epithelial function or alter immune cell profiles. However, the potential therapeutic impact of corneal rewetting on the stromal compartment in dry eye is unknown.

To test the impact of corneal rewetting on the stroma, we employed the *Aire* knockout (Aire KO or KO) mouse model of autoimmune disease that results in lacrimal gland degeneration and aqueous deficient dry eye. This model exhibits key pathologies of human autoimmune-mediated disease, including chronic disruption of corneal epithelial integrity, reduced innervation, loss of barrier function, and altered stromal cells.[13,15,16] Similar to human patients, the prevalence and severity of dry eye development in female *Aire* KO mice greatly exceeds that of their male littermates beginning with a moderate reduction in tear secretion and corneal barrier dysfunction, that can progress to severe aqueous deficiency and significant pathologies affecting the corneal epithelium and sensory nerves by 7 weeks.[13] We have previously shown that PBS is not sufficient to restore tear production, epithelial integrity, sensory innervation, barrier function, or suppress inflammation.[3] However, the response of the stroma and BM to rewetting has not been tested.

To define changes in the KO corneal stroma in response to intermittent rewetting, we performed immunofluorescent imaging of stromal collagen fibers in KO mice, treated with or without PBS three times per day for 14 days and compared them to wild type (WT) controls (Figure 1A). Unlike the densely packed, uniformly aligned, narrow collagen 1 fibers lying parallel to the corneal surface in WT mice, the desiccated KO tissue displayed a profound increase in disoriented fiber angles (>40–90°, Figures 1B, 1C, S1A, and S1B) and fiber thickening (Figures 1B and 1D)). Stromal collagen fiber organization and three-dimensional ultrastructure, including fiber alignment and spacing, play essential roles in optical transparency.[17] Transmission electron microscopy (TEM) of cross-sectioned corneal stroma revealed significant disruption to collagen fibril organization in KO mice (Figures 1E, 1F, and S1D). To quantify fibril orientation complexity, we applied a structure tensor-based analysis to TEM images, computing a Shannon entropy score and fiber fraction from the local orientation distribution of each image. In WT corneal stroma, over 60% of fibrils were aligned toward the predominant vertical axis with no substantial secondary orientation peaks, reflecting a highly organized lamellar architecture. In contrast, KO stroma exhibited a marked increase in orientational diversity, with only 35% of fibrils aligned vertically and a broad spectrum of fibril angles distributed across the remaining population, indicative of lamellar disorganization. We also observed increased interfibrillar spacing in KO corneas (Figures 1G and 1H), consistent with stromal edema and in line with the increased stromal thickness measured in these animals (Figure 1C). Notably, PBS treatment restored stromal architecture toward a WT-like state, with over 70% of fibrils realigning toward the vertical axis, a marked reduction in orientational entropy, and interfibrillar distances closely resembling those of WT controls (Figures 1F and 1H). The process of realignment was initiated within the first day of PBS application, as shown by the substantial rescue of expression of a large cohort of ECM-associated genes, such as fibronectin (Fn), decorin (Dcn), lumican (Lum), and numerous collagens (e.g., Col4a3, Col12a1) at 24 h after treatment (Figure S1E).

These data suggest PBS treatment is sufficient to promote the restoration of stromal integrity, as well as cell-matrix interactions vital for corneal wound healing, transparency, and visual acuity.

Keratocytes possess extensive plasticity and undergo regenerative transformation in response to corneal rewetting

Single cell analyses of healthy murine and human cornea show heterogeneity in stromal keratocytes under homeostatic conditions.[7,18] Although keratocytes are known to shift from a resting to an activated state following injury, specific changes in their cell states under pathological or healing conditions and the mechanisms driving these changes, remain unknown. To investigate keratocyte identity and cell state transitions in WT, KO, and KO + PBS, we performed single-nuclei RNA-seq (snRNA-seq) to characterize transcriptional profiles and associated signaling pathways (Figure 2A). snRNA-seq of whole corneas (n = 5, 10 corneas per group) yielded 67,117 single nuclei that were classified into the different cell types that constitute the cornea, including keratocytes, epithelial cells, immune cells, and endothelial cells (Figure S2A). Consistent with our previous findings,[3] immune cells were greatly expanded in both KO and KO + PBS samples. To resolve stromal keratocyte heterogeneity, we employed a two-step analytical approach. In the first step, epithelial, immune, and endothelial populations were identified based on established lineage markers and removed from the stromal analysis. The remaining stromal cells were identified as keratocytes based on their expression of extracellular matrix (ECM) genes characteristic of the keratocyte transcriptional program, including *Col1*, *Dcn*, and *Lum* identifying 3153 WT, 5123 KO and 3558 KO + PBS keratocytes. In the second step, unbiased subclustering (R package, Seurat) was performed within this isolated keratocyte population, defining 10 keratocyte

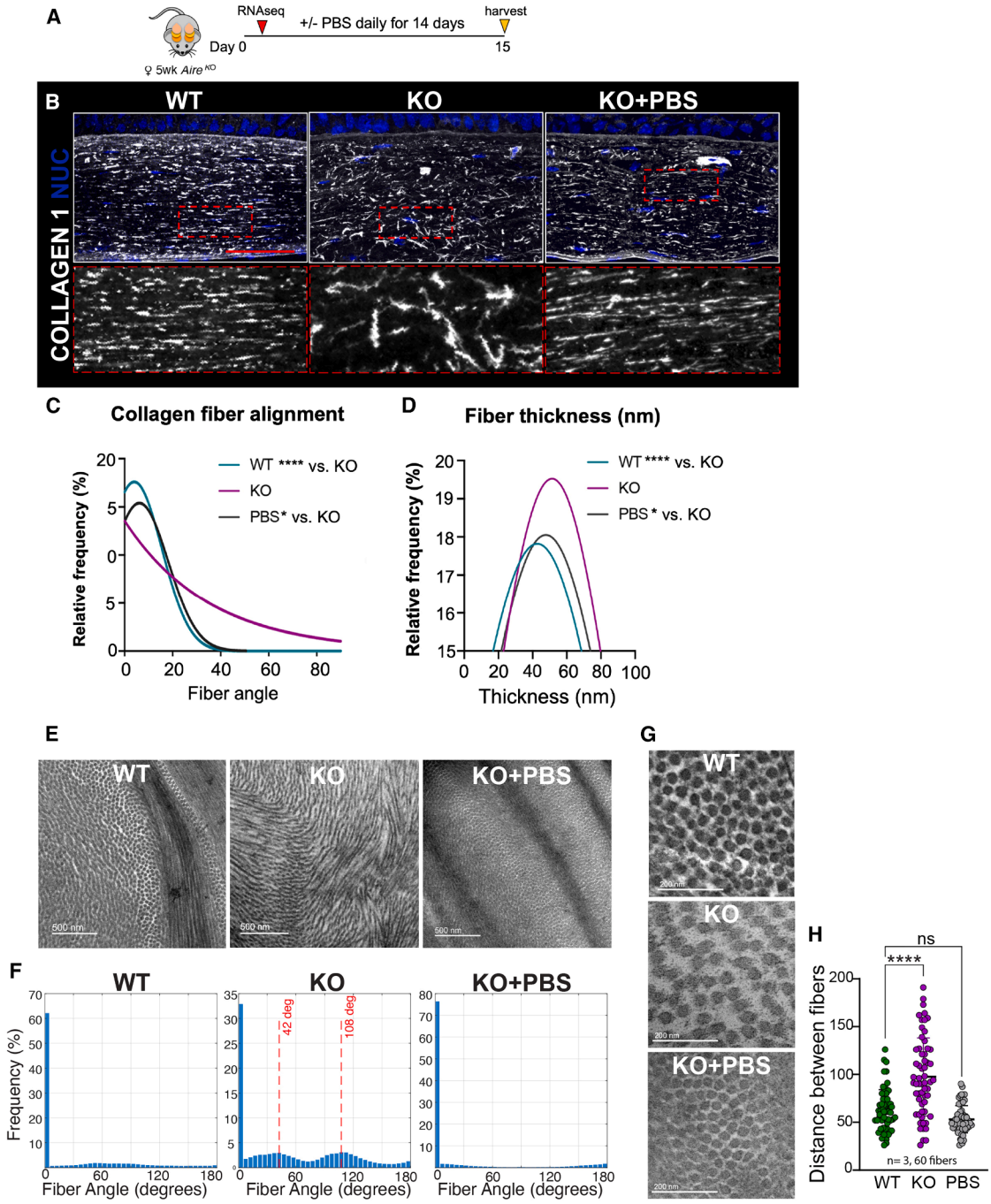

Figure 1. Topical rewetting of the ocular surface promotes stromal regeneration

(A) Schematic of treatment regimen showing (top).

(B–D) Immunofluorescent imaging of stromal collagen 1 organization in healthy, KO and KO + PBS cornea. Quantification of collagen fiber alignment relative to the BM and collagen 1 fiber thickness (C) in the corneal stroma of each group.

(E and F) Representative transmission electron microscope (TEM) images of stromal collagen fibrils in each group and corresponding fiber orientation distribution. Red dash lines indicate the peak orientation angles in KO corneas. Fibrils aligned toward the predominant vertical axis are defined as 0°.

(G and H) Higher-magnification TEM images of each group illustrate fibril packing organization and interfibullar distance, with quantification shown in H. NUC = nuclei. Scale bars: B, 50 μm E, 500 nm and G, 200 nm. *$p < 0.05$; **$p < 0.01$; ***$p < 0.001$; ****$p < 0.0001$. Data in C and D were subjected to Kolmogorov-Smirnov test. Data in H were analyzed using a one-way analysis of variance with a Tukey's post-hoc test. Each dot in the bar graph represents one individual fibril measurement with 40 fibrils measured per sample, $n > 4$ mice per group. Error bars represent standard deviation.

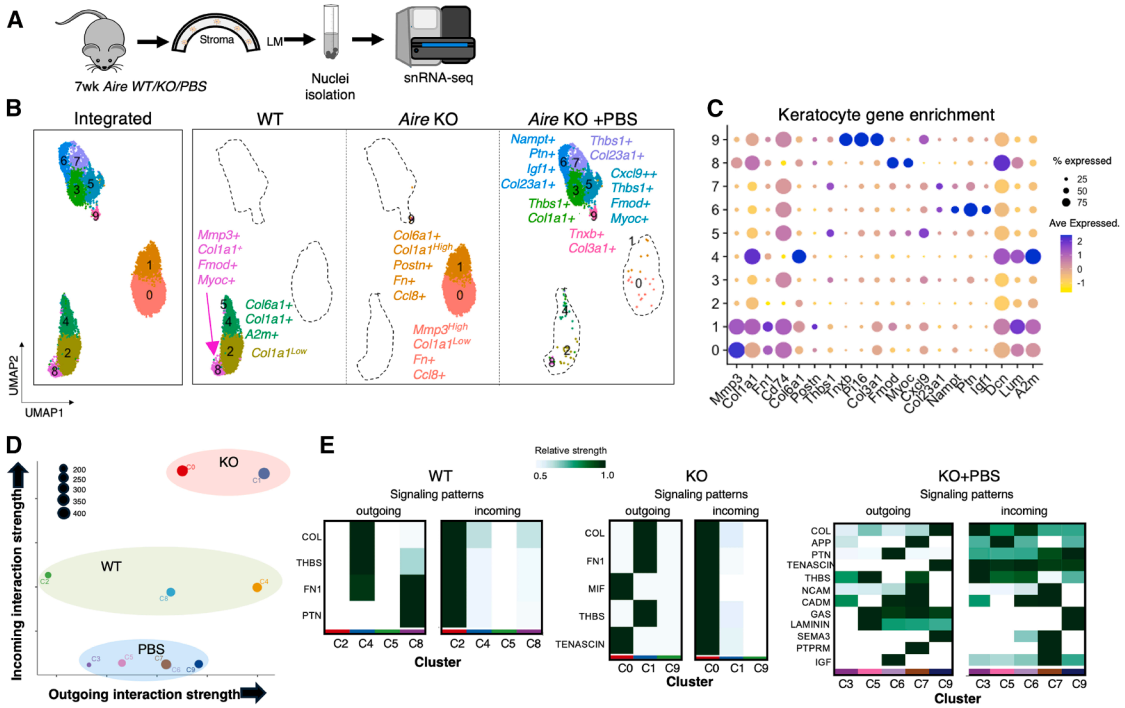

Figure 2. Stromal keratocytes in the diseased cornea exhibit striking plasticity in response to disease and rewetting

(A) Experimental and analytical workflow. Corneal stroma from WT, Aire KO, and KO + PBS mice were isolated, nuclei were extracted, and single-nucleus RNA sequencing (snRNA-seq) was performed.

(B) Integrated UMAP projection of stromal keratocytes from WT, Aire KO, and KO + PBS corneas showing distribution into 10 transcriptionally distinct clusters. Individual UMAP plots display the distribution of keratocytes within each condition, with representative marker genes highlighting the identity of each cluster.

(C) Dot plot showing enrichment of representative marker genes across keratocyte clusters.

(D) Scatterplot summarizing predicted intercellular communication patterns among keratocyte clusters inferred by Cell Chat. visualizing dominant senders and receivers of cellular signals in a 2D space. Each point represents a keratocyte cluster, positioned according to total outgoing (*x* axis) and incoming (*y* axis) signaling probabilities that predominately act as signal senders and receivers.

(E) Heatmaps showing significantly signaling pathways contributing most strongly to outgoing or incoming communication for keratocyte clusters within each condition (WT, KO, and KO + PBS). Color intensity reflects relative signaling strength predicted by CellChat.

subpopulations (Figures 2B, 2C, S2B, and S2C), with each treatment group comprising multiple distinct cell clusters.

WT corneas were primarily composed of 3 clusters (clusters 2, 4, 8). Cluster 4 (28%) was enriched in ECM component genes (*Col6al* and *Col1a1)* and cluster 8 (10%) expressed genes associated with matrix remodeling such as matrix degrading enzyme *Mmp3*, a key player in ECM remodeling, *and Fmod*, a proteoglycan critical to generation of corneal transparency[19] and scarless wound healing in skin[20] through collagen fibrillogenesis, suggestive of active keratocytes. In comparison, cluster 2 (62%) was restricted to low levels of *Col1a1*, the major collagen within the bulk of the fibrils, suggesting these cells have reduced physiological function and as such, are ‘‘resting’’ keratocytes.

In the KO cornea, keratocytes segregated into two clusters (cluster 0, 1) that were dramatically different from WT. Unlike the ‘‘resting’’ or ‘‘active’’ keratocyte clusters in the WT, both KO clusters were enriched in inflammatory and injury associated genes such as *Ccl8*, *Cd74*, *and Slpi*, as well as in fibronectin (*Fn1*) (Figures 2B and 2C), a factor highly associated with chronic injury.[21] In addition, cluster 0 (61%) was highly enriched in *Mmp3*, and cluster 1 (39%) in periostin (*Postn*), a marker of pro-fibrotic fibroblasts in chronic injury conditions,[22] suggestive of enhanced matrix turnover and inflammatory signaling.[23]

Strikingly, rewetting further modified keratocyte cell states resulting in five unique clusters (clusters 3, 5, 6, 7, and 9) that were specifically enriched in genes associated with wound repair. Clusters 3 (36%), 5 (25%), and 7 (15%) were enriched in *Thbs1*, a matricellular protein released and/or secreted following tissue injury that is typically associated with ECM organization[24,25] and inhibiting angiogenesis.[26] Clusters 6 (18%) and 7 were enriched in *Col23a1*, a non-fibrillar collagen involved in cell-cell and cell-matrix adhesion.[27,28] Cluster 6 was also enriched for *Igf1*, which has been shown to support corneal epithelial wound healing,[29,30] and pleiotrophin (*Ptn*), a factor with neurotrophic activity that promotes nerve regeneration and is actively engaged in bone marrow stromal cell-mediated regeneration.[31] Cluster 9 (4%) was strongly enriched in matrix proteins such as *Tnxb* which is found in the peripheral but not central stroma[32,33] and provides structural support and regulates collagen architecture and tissue elasticity.[34–38] Additionally, the peptidase inhibitor *Pi16*, which is highly expressed in stromal/fibroblast stem-like cells across various tissues[39] was also

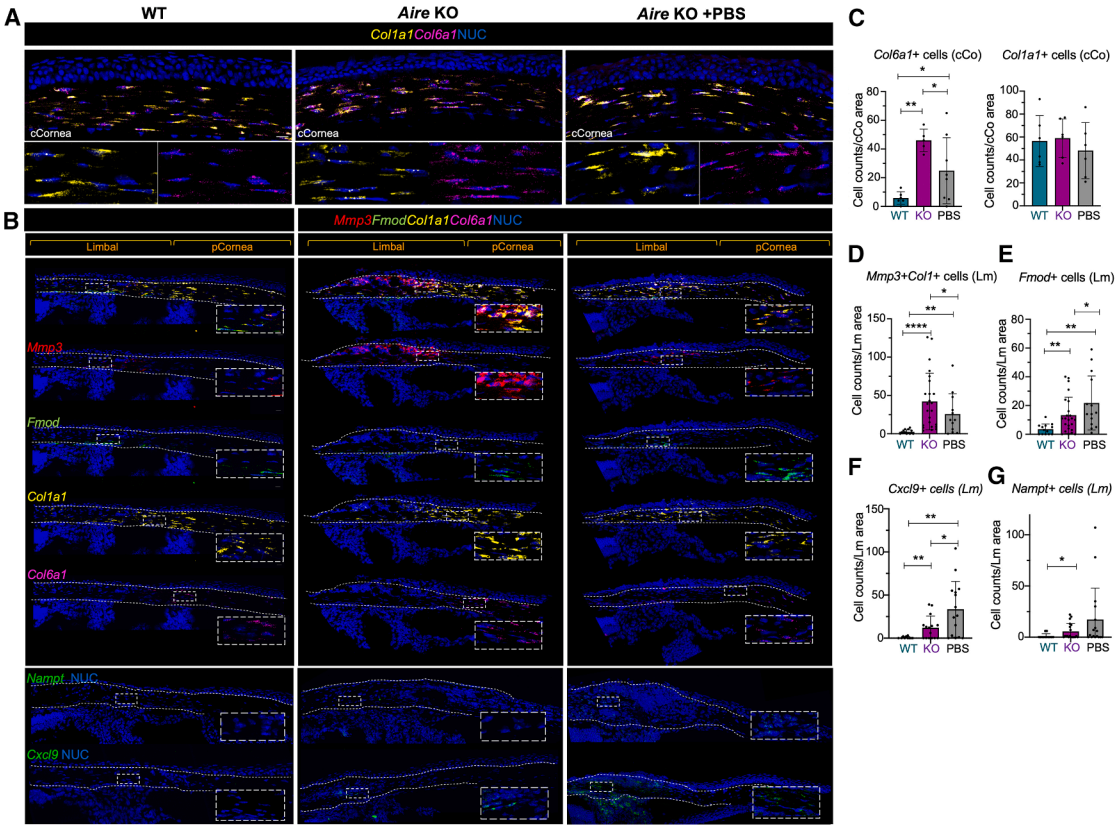

Figure 3. Corneal rewetting promotes a reparative response in the diseased stroma by depleting cells associated with excessive ECM remodeling and enriching for those promoting wound healing

(A and B) RNAscope *in situ* hybridization showing spatial localization of marker genes corresponding to keratocyte clusters in the central cornea (A, cCornea) and peripheral cornea and limbal region (B, pCornea and limbus). Boxes indicate higher-magnification views of stromal cells within the corneal stroma. Dotted lines outline the upper and lower boundaries of the stromal compartment.

(C–G) Quantification of keratocytes expressing high transcript levels of the indicated marker genes across the 3 groups. *$p < 0.05$; **$p < 0.01$; ***$p < 0.001$; ****$p < 0.0001$; Data in C–G were analyzed using a one-way analysis of variance with a Tukey's post-hoc test. Each dot in the bar graph represents one biological replicate. Error bars represent standard deviation. $n \geq 4$ mice per group. Scale bars, 50 μm.

enriched, suggesting that Pi16 may also mark highly plastic keratocytes.

Consistent with the apparent therapeutic benefit of corneal rewetting relative to the untreated KO, there also were no cell clusters enriched in pro-fibrotic or chronic injury markers such as *Col6a1* or *Mmp3* in the PBS-treated cornea, supporting the pro-regenerative state of the tissue (Figures 2B and 2C).

Tissue homeostasis and repair are complex processes involving activation of various signaling pathways and intercellular coordination. Through analysis of intercellular communication networks via CellChat,[40] we identified differences in cell signaling between clusters in each condition that were consistent with the marker genes. In the WT cornea, clusters 4 and 8 showed active signaling to the surrounding cells such as COLLAGEN, THBS, and FN1 signaling, while cluster 2 was the main receiver of cellular signaling (Figures 2B, 2D, and 2E). The two KO cell clusters exhibited the greatest levels of active incoming and outgoing signaling networks among all the keratocyte clusters including inflammatory signaling-MIF and TNX that were not seen in the WT (Figure 2D). Comparison of the intercellular communication networks between the two KO clusters indicated cluster 0 is the main receiver of incoming cellular signaling as well as the source of outgoing inflammatory signaling-MIF, suggestive of an activation of an autocrine inflammatory loop within these keratocytes (Figure 2E). CellChat analysis further revealed 5 unique clusters as key sources of THBS, PTN, IGF, and TENASCIN signaling in the re-wetted keratocytes (Figure 2E), supportive of their reparative/regenerative role. The observed increase in complexity of the intercellular communication network further illustrates reparative actions of the keratocytes in the re-wetted cornea (Figure 2E). Together, our data reveal the dynamics of keratocyte cell state under homeostatic, diseased, and wetted settings and that rewetting the cornea may produce a reparative keratocyte phenotype.

We next validated the different clusters of keratocytes and identified their spatial locations within the cornea through *in situ* hybridization (RNAscope HiPlex) and immunofluorescent analysis (Figure 3). In the WT, we found that the abundant *Col1a1* enriched cells (cluster 2) were distributed throughout the corneal stroma, consistent with the corneal-wide array of

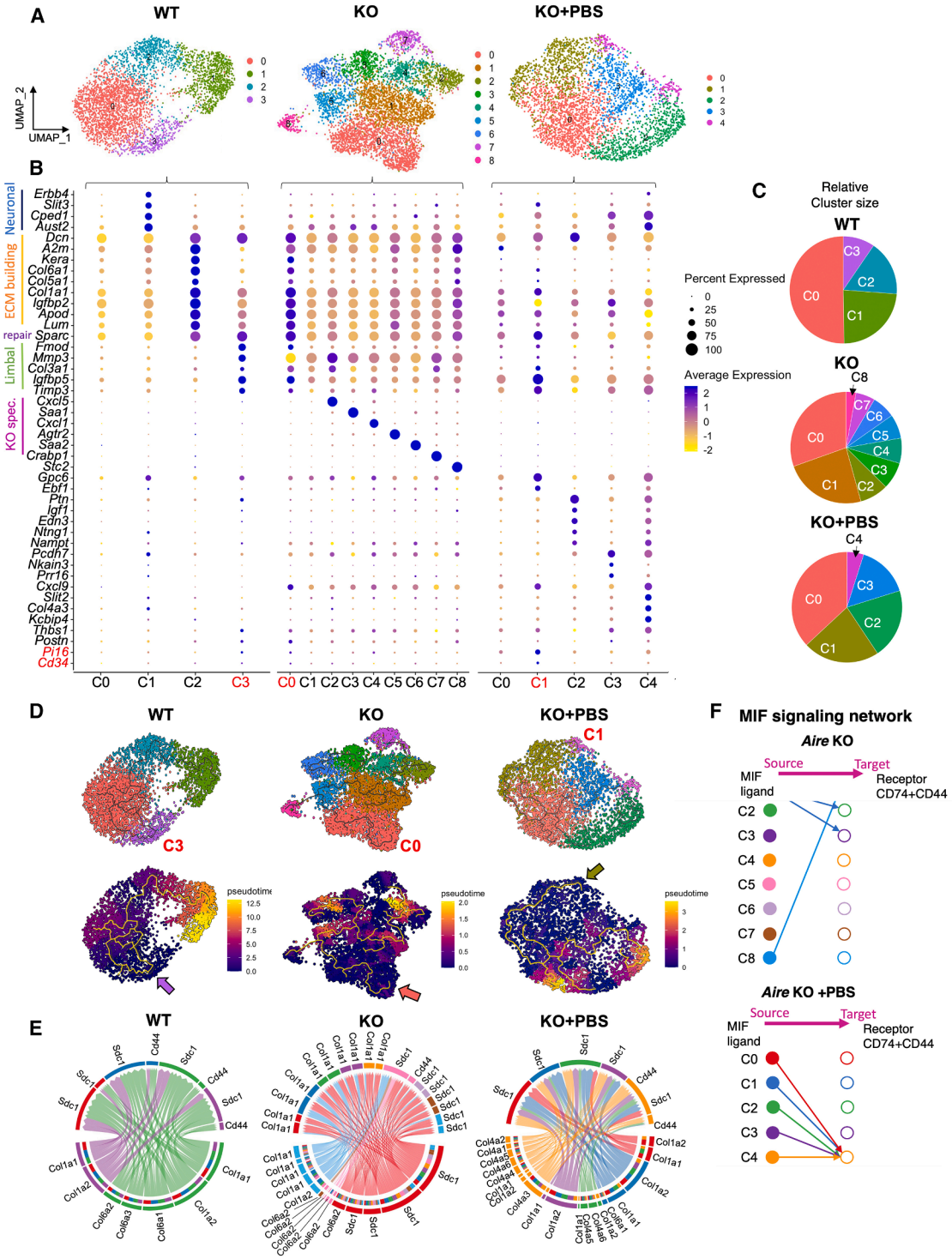

Figure 4. Keratocytes transition from inflammatory to regenerative transcriptional states following corneal rewetting

(A–B) UMAP projection (A) and corresponding dot plot (B) illustrating the transcriptional heterogeneity of keratocytes within each condition and the marker genes associated with each identified cluster. The size of each dot corresponds to the percentage of cells within the cluster expressing the gene, The average expression level for the listed genes is indicated by the color scale.

(C) Pie charts summarizing the relative proportion of keratocytes assigned to each cluster across the three experimental conditions (WT, KO, and KO + PBS).

(D) Monocle trajectory inference and pseudotime analysis illustrating predicted transitions between keratocyte transcriptional states within each condition. Dark purple represents earlier states, while yellow represents later states. Arrows indicate the inferred trajectory starting point.

(legend continued on next page)

collagen fibers and their known enrichment in COL1 (Figures 3A and 3B). Clusters potentially involved in ECM remodeling (cluster 4 and 8), were located within the limbal and peripheral regions of the cornea. Specifically, *Col6a1*+ cells (cluster 4) were most abundant in the peripheral cornea (Figures 3A, 3B, and S3A), suggesting a potential role of these cells in forming distinct networks of microfibrils. A small proportion of WT keratocytes (cluster 8) enriched in *Fmod*, key regulator of collagen organization, and ECM remodeler *Mmp3* were concentrated at the limbal region (Figure 3B), suggesting this population is involved in maintaining stromal architecture during homeostasis.

Similar to WT, cells enriched in *Col1a1* and *Col6a1* in the KO were distributed across the peripheral and central cornea with very few *Col6a1*+ cells located in the limbal region (Figures 3A and 3B). However, the number of *Col6a1*^{high} keratocytes in the KO was significantly greater than WT while numbers of *Col1a1*^{high} keratocytes remained relatively unchanged (Figures 3A and 3C). Although COL6 is a nonfibrillar collagen that plays an important role in wound healing and tissue repair,[41,42] excessive production of COL6 is often associated with tissue fibrosis[43] suggesting that an expansion of this population in the KO impairs effective wound healing. Similar to the WT keratocytes that were enriched in *Mmp3* and *Fmod* (cluster 8), KO *Mmp3*+ (cluster 0) and *Fmod*+ keratocytes (cluster 1) were specifically found in the limbal region in close association with infiltrating immune cells (Figure 3B). Strikingly, the number of these cells at this location dramatically increased with disease (Figures 3B–3E), consistent with the size of *Mmp3*-enriched cluster 0 and *Mmp3* expression level (Figures 2B and 2C), suggesting excessive ECM remodeling and aberrant wound healing were taking place in the limbal region.

We next validated the presence of the potentially regenerative clusters enriched in the rewetted cornea. *Thbs1*+ keratocytes (clusters 3, 5, and 7) were located throughout the corneal stroma, consistent with THBS1 being essential for avascularity and transparency as well as accelerated wound healing in the corneal epithelium[26,44] (Figure S3B). Cells enriched in *Nampt*, a protein shown to protect cells from apoptosis[45] (cluster 6), and chemokine (C-X-C motif) ligand 9 (*Cxcl*9), an immune modulator[46] (cluster 5), were localized to the limbal stroma (Figures 2B, 2C, and 3B–3G). In addition, in the re-wetted cornea, the population of *Col6a1*^{high} and *Mmp3*^{high} keratocytes was greatly reduced (Figures 3A–3D) while *Fmod*^{high} expressing keratinocytes were increased (Figures 3B and 3E), potentially indicating the reversal of excessive ECM remodeling and the transition of these keratocyte populations to a reparative state. In summary, our data reveal the plasticity of keratocytes and their extensive remodeling in response to disease and treatment through corneal rewetting.

Keratocytes transition from an inflammatory to a regenerative state in response to corneal rewetting

To gain a deeper understanding of the heterogeneity and intercellular relationships under each condition, we analyzed the WT, KO, and KO + PBS datasets separately and performed additional sub-clustering of keratocytes (Figure 4A). Cluster identities were evaluated using established keratocyte markers, including *Kera* (Keratocan), *Lum*, and *Dcn*, which are shown in the marker expression map (Figure 4B) and confirm the keratocyte identity of the analyzed stromal populations. This analysis revealed distinct keratocyte subpopulations in each condition, defined by differential gene expression patterns in conjunction with known cell state identifiers (Figures 4A–4C). In the WT cornea, four keratocyte clusters were identified. Cluster 0, the largest population (>50%), exhibited relatively low expression of decorin and collagen transcripts and was therefore designated as a putative resting keratocyte population. Cluster 1 (23.57%) was highly enriched for a set of genes previously associated with neuronal signaling or axon guidance, including *Erbb4*, *Slit3*, *Cped1*, and *Auts2*, suggesting the potential involvement of corneal nerves. Cluster 2 (16.64%) showed elevated expression of ECM genes, consistent with a role in ECM maintenance or remodeling during corneal homeostasis. Cluster 3 (9.56%) was enriched for limbal-associated markers such as *Fmod* and *Mmp3*, indicating preferential localization to the limbal region (Figures 4B and 4C). Notably, a small subset of cells within cluster 3 were enriched in cell state plasticity-related genes including *Pi16,* a marker of fibroblast precursors and stromal cell plasticity[39] and *Cd34,* a marker of diverse populations of progenitor cells[47,48] known to be expressed by human cornea stromal cells[49] (Figure 4B).

In contrast, keratocytes from the inflamed, desiccated KO cornea segregated into nine clusters, reflecting increased transcriptional heterogeneity (Figure 4A). The putative resting keratocyte population (cluster 1) was strongly reduced in the KO cornea (23.85%) compared to WT (cluster 0, 50.23%), whereas an ECM-associated cluster was expanded (KO cluster 0: 30.45% vs. WT cluster 2: 9.56%) (Figures 4A and 4C). Consistent with active tissue repair, KO cluster 0 was enriched for *Sparc*, a gene associated with corneal wound healing[50] and stromal remodeling.[51] Markers associated with ECM regulation and cell-matrix interactions, including *Fmod* and *Igfbp5*, both enriched in the limbal stromal region (Figures 3B and 3C), as well as *Postn*, which is upregulated in response to corneal injury,[52] were distributed across clusters 0 and 2. In contrast, *Mmp3*, a matrix-degrading enzyme expressed by limbal keratocytes (Figures 3B–3D) was largely confined to cluster 2. Enriched expression of *Pi16* and *Cd34,* markers associated with enhanced stromal plasticity, was predominantly restricted to cluster 0, suggesting this population may retain features of a progenitor- or niche-associated keratocyte state.

Notably, gene signatures associated with neuronal interactions observed in WT keratocytes were largely absent in KO keratocytes. Instead, clusters 2 through 8 each exhibited enrichment for distinct immune- or inflammation-associated genes (Figure 4B, KO dot plot). These included *Cxcl5* (cluster 2), which

(E) Chord diagrams depicting collagen signaling networks inferred by CellChat, showing predicted ligand-receptor interactions between keratocyte clusters under each condition.

(F) Comparison of macrophage migration inhibitory factor (MIF) signaling networks and associated ligand-receptor interactions between keratocyte clusters in KO and KO + PBS corneas.

plays a role in recruiting lymphocytes and eosinophils during an immune response[53]; *Saa1* (cluster 3), an inducer of inflammatory gene expression in fibroblasts[54]; *Cxcl1* (cluster 4), a chemoattractant cytokine that primarily recruits neutrophils[55]; *Agtr2* (cluster 5) mediates tissue fibrosis signaling in activated fibroblasts[56]; *Saa2* (cluster 6), amplifies innate immune responses[57]; *Crabp1* (cluster 7), marks wound-healing fibroblast[58]; and *Stc2*, which was exclusively enriched in the smallest population (cluster 8 (2.86%)), and has been reported to limit $CD8^+$ T cell recruitment and regeneration,[59] consistent with a potential immunomodulatory role. Together, these enrichments suggest that KO keratocytes adopt diverse immune-modulatory or stress-associated transcriptional states, reflecting heightened plasticity in response to chronic injury, though functional validation will be required to confirm these inferred roles.

Following PBS treatment, keratocyte heterogeneity was reduced compared to KO, with five distinct clusters identified (Figures 4A–4C). The relative abundance of the putative resting keratocyte cluster increased (C0, 37%) compared to untreated KO corneas (C0, 24%). An ECM-associated cluster (C1) expressing *Kera*, *Lum*, and *Col6a1*, was reduced relative to untreated KO corneas (PBS (C1): 23.41% vs. KO (C0-8): 30.45%) while clusters 2 to 4 (together comprising 40% of keratocytes) were enriched for genes previously linked to wound repair and regeneration, including *Ptn*, *Igf1*, *Thbs1*, and *Col4a3*.[60] Limbal-associated markers (*Mmp3* and *Fmod)* were distributed across clusters C1 and C3, whereas *Pi16* and *Cd34* expression remained restricted to the ECM remodeling cluster (C1), together with *Sparc*. Additionally, expression of neuronal-associated markers observed in WT keratocytes (C1), including *Slit3 and Erbb4*, was partially restored following rewetting, albeit with broad expression across multiple clusters (Figure 4B), consistent with the re-emergence of gene signatures associated with nerve-stromal interactions. Collectively, these transcriptional shifts are consistent with a redistribution of keratocyte states following rewetting, favoring gene-expression programs associated with tissue repair.

To investigate the potential relationships among keratocyte subclusters under homeostatic, disease, and regenerative conditions, we conducted lineage trajectory analysis inference using monocle 3 (Figure 4D). The predicted trajectories revealed substantial keratocyte plasticity, with cells occupying multiple interconnected transcriptional states rather than following a single linear differentiation path. In the KO cornea, cells from the putative resting keratocytes cluster (C1) were predicted to transition toward an ECM-remodeling or inflammatory-associated state through intermediate clusters (Figure 4D, upper). Pseudotime analysis anchored to the limbal-associated population (C0, arrows) revealed a linear trajectory culminating in the neuronal-associated cluster in the WT cornea, placing this state at a later differentiated stage relative to other clusters (Figure 4D, lower). However, no dominant or clear trajectory was found in the KO or PBS-treated conditions, consistent with increased keratocyte state plasticity during inflammation and repair. While these analyses are predictive, they support a model in which keratocytes dynamically adapt their transcriptional programs in response to inflammatory and regenerative cues.

To compare predicted intracellular communication among keratocyte clusters across conditions, we conducted CellChat analysis to infer potential sources and targets of signaling pathways based on ligand and receptor interactions. Across all three conditions, collagen signaling emerged as the most enriched pathway in keratocytes, however, the specific collagen types involved and their predicted expression patterns differed markedly between groups (Figure 4E). In WT and untreated KO corneas, keratocytes broadly expressed the collagen receptors *Cd44* and *Sdc1*, while a subset of ECM-associated clusters (C2 in WT and C0 in KO, potential ECM building states) were predicted to be the primary producers of collagens 1 and 6. In the untreated KO, additional clusters (C5, C8) were also predicted to contribute to collagen 1 and 6 production, consistent with an overall increase in collagen signaling. This expansion of *Col6a*^{high} keratocytes was independently supported by immunofluorescent analyses in the KO cornea (Figures 3A–3C), in line with a pro-fibrotic environment. In contrast, PBS-treated corneas exhibited a broader distribution of collagen production across keratocyte clusters, accompanied by a predicted downregulation of *Col6* and relative enrichment of *Col4*, which is essential for BM rebuilding. These shifts are consistent with altered ECM remodeling dynamics following rewetting and suggest a transition toward a tissue state supportive of repair. Under PBS treatment, all keratocyte clusters were predicted to express the collagen receptor *Sdc1*, whereas co-expression of *Cd44* in WT and KO corneas, was restricted to a single cluster (C4). CD44 is a multifunctional cell-surface receptor involved in a range of cellular processes including cell adhesion, migration, inflammation, and wound repair.[61] Thus, the reduced prevalence of Cd44-expressing *Sdc1*+ keratocytes following rewetting may reflect attenuation of inflammatory signaling within the stromal compartment (Figure 4E).

One of the more notable differences in predicted cell-cell communication identified by CellChat involved the macrophage migration inhibitory factor (MIF) pathway, which was predicted to be enriched in KO keratocytes (Figure 4F). MIF is known to be upregulated in inflamed tissues and to signal through the co-receptors, CD44 and CD74, both of which are required for signaling.[62,63] In untreated KO, the MIF1 ligand was primarily predicted to be produced by clusters C1 (~24%) and C8 (~3%), while C0-C3, together comprising ~60% of the keratocytes, were predicted to act as signal recipients through co-expression of both CD74 and CD44. In comparison, while MIF ligand expression was broadly detected in PBS-treated keratocytes, co-receptor expression more restricted, with only the small cluster C4 (4%) predicted to express both co-receptors (Figure 4F). These patterns are consistent with an overall attenuation of MIF signaling following PBS treatment and suggest that corneal rewetting may dampen inflammatory signaling in keratocytes.

Interestingly, PBS-treated keratocytes within cluster C4 were also predicted to be enriched for neuronal- and BM-associated genes, raising the possibility that this population may represent a reparative or transitional state. In addition to its established role in inflammation, MIF has been implicated in wound repair through regulation of repair- and inflammation-associated genes, including *Col1a1*, *Cxcl10*, and *Thbs1*, suggesting that

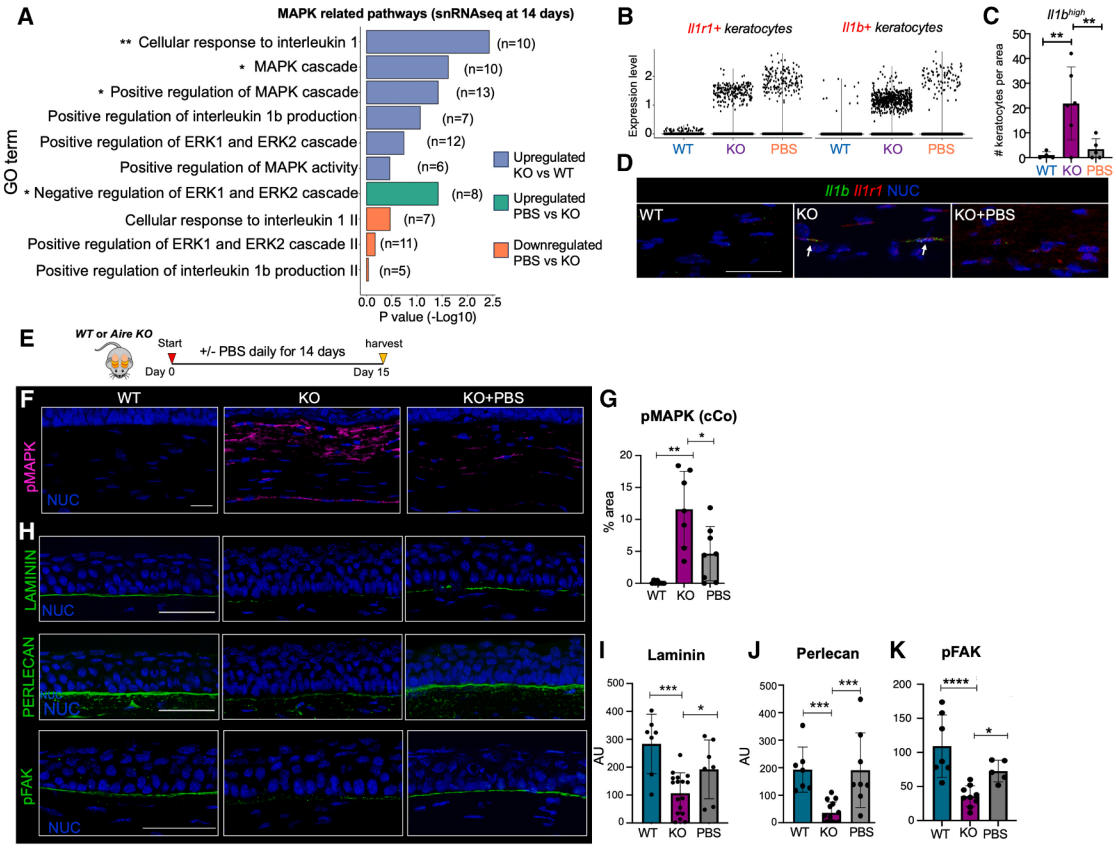

Figure 5. Corneal rewetting dampens stromal IL1β-MAPK signaling and restores stromal and basement membrane integrity

(A) Gene ontology (GO) enrichment analysis of differentially expressed genes identified from the snRNAseq datasets. *n* = number of significant differentially expressed genes associated with each pathway.

(B) Violin plots comparing *Il1r1* and *Il1b* expressing cells within the corneal stroma of WT, KO, and KO + PBS groups. Each dot represents an individual cell.

(C and D) Immunofluorescent analysis of IL1β-expressing cells, (C) and quantification of *Il1b* ^{high} keratocytes (D) within the cornea stroma of WT, KO, and KO + PBS groups.

(E) Schematic of the topical treatment regimen (14 days beginning at 5 weeks of age).

(F–K) Immunofluorscent analysis (F, H) and quantification (G, I, J, K) of phosphorylated MAPK (pMAPK) (F, G), laminin (H, I), perlecan (H, J) and pFAK (H, K) within the central cornea of WT, KO and KO + PBS groups.

NUC = nuclei. Scale bars, 50 μm *$p < 0.05$; **$p < 0.01$; ***$p < 0.001$; ****$p < 0.0001$; Bar graphs in C–K were analyzed using one-way analysis of variance with a Tukey's post-hoc test. Each dot represents one biological replicate. Error bars represent standard deviation. n ≥ mice per group.

MIF signaling could contribute to the functional properties of this cell cluster. Collectively, these findings suggest that keratocytes may exhibit considerable plasticity in response to inflammatory cues, with the capacity to shift toward states associated with tissue repair.

Corneal rewetting is associated with attenuation of MAPK-related signaling, potentially in response to IL1, recovery of the stroma and BM and generation of pro-repair keratocytes

To gain mechanistic insight into the rescue of stromal integrity following corneal rewetting, we performed gene ontology (GO) analysis of our snRNAseq datasets. This analysis revealed KO keratocytes to be significantly enriched for pathways associated with interleukin signaling, and more specifically IL1β-related processes (Figure 5A). IL1β is a well-established mediator of autoinflammatory responses and contributes to multiple local inflammatory features including activation of the MIF pathway by upregulating MIF ligand expression[64] and MMP synthesis to drive ECM proteolysis.[65,66] It can also trigger a positive inflammatory feedback loop that amplifies the IL-1 response through autocrine or paracrine signaling in keratocytes.[67,68] This can promote tissue regeneration under acute conditions but leads to chronic disruption with persistent injury.[69] We previously showed that *Il1β* and its primary receptor *Il1r1* are upregulated in Aire KO cornea,[70] implicating IL1 signaling in dysregulated stromal homeostasis under desiccating conditions.

Analysis of snRNA-seq data revealed that the proportion of *Il1r1*^{high} keratocytes was not reduced following corneal rewetting compared to untreated KO (WT = 0%, KO = 4%, PBS = 5%). In contrast, the fraction of *Il1b*-expressing keratocytes was markedly elevated in the KO cornea (10.7%) relative to WT (0.3%) and was reduced following PBS treatment (2.7%) (Figures 5B–5D). RNAscope analysis at 14 days further

supported these findings, demonstrating an abundance in Il1b^{high}Ilr1-expressing keratocytes in the KO stroma compared to WT, which was significantly reduced with PBS treatment (Figures 5C and 5D).

Signal propagation by IL1β mainly depends on mitogen-activated protein kinases (MAPKs specifically ERK). Pathway analysis of the snRNA-seq data revealed MAPK signaling programs were strongly elevated in KO keratocytes and were predicted to be reduced following PBS treatment at 14 days (Figure 5A). Consistent with these transcriptional trends, immunofluorescent analysis revealed a profound increase in pMAPK expression throughout the KO stroma that was dramatically reduced by corneal rewetting (Figures 5E and 5F). While these findings do not establish direct causal suppression of MAPK signaling by PBS treatment, they support an association between rewetting and reduced activation of IL1-MAPK-related signaling in stromal keratocytes.

Previous studies have shown that IL1b stimulation and MAPK signaling pathway activation occur in mouse models of experimentally induced dry eye,[71] resulting in upregulation of BM-degrading enzymes including MMPs such as MMP3 and MMP9.[72] These enzymes degrade a variety of BM components required to maintain corneal epithelial barrier function and stromal-epithelial communication. As BM integrity is critical for epithelial homeostasis and regeneration, disruption of this structure impairs epithelial repair[73]

Given our snRNA-seq and immunofluorescent data showing enrichment of ECM remodelers and upregulation of MAPK signaling in KO inflammatory keratocytes (Figures 2, S2, and S3), we next assessed BM integrity in untreated and PBS-treated KO corneas. In untreated KO corneas, the BM was significantly compromised, as evidenced by the severe depletion of two key BM proteins, laminin, and perlecan.[74] In contrast, PBS treated KO corneas exhibited restoration of laminin and perlecan to levels comparable to WT controls (Figures 5E–5I). Reestablishment of the BM with PBS was also accompanied by increased epithelial cell adhesion essential to epithelial regeneration. In untreated KO corneas, phosphorylated focal adhesion kinase (pFAK), the active form of a mechanosensor that accumulates at epithelial-BM adhesion sites and is required for epithelial-matrix interactions during wound healing,[75] was nearly absent compared to WT corneas (Figures 5E–5I). However, following PBS treatment pFAK levels were restored, suggesting recovery of epithelial-matrix adhesion and ECM-associated mechanical signaling.

Together, these data suggest that corneal rewetting is associated with reduced MAPK-related signaling and restoration of BM integrity in the desiccated cornea. While these data do not establish direct mechanistic causality, they support a model in which rewetting alleviates inflammatory stromal states, potentially downstream of IL1 signaling, thereby promoting stromal recovery and BM repair through the emergence of keratocyte states permissive for tissue regeneration.

DISCUSSION

Dry eye disease has been predominantly characterized as a disorder of the ocular surface epithelium, while the contributions of the underlying corneal stroma and BM, both essential for epithelial repair, remain comparatively understudied. The present study addresses this gap by examining stromal changes in a mouse model of spontaneous, aqueous-deficient dry eye and evaluating the therapeutic potential of corneal rewetting. Our findings demonstrate that in addition to its detrimental impact on corneal epithelial integrity, aqueous tear deficiency causes substantial disruption of stromal organization and BM deposition and marked alterations in stromal keratocyte populations. Using single-cell RNA sequencing, we identified distinct keratocyte subpopulations that adopt inflammatory phenotypes under aqueous-deficient conditions. Rewetting the cornea three times daily with PBS largely restored BM integrity, stromal collagen organization and shifted keratocyte populations from inflammatory states toward less inflammatory and potentially reparative phenotypes. These stromal and cellular changes occurred despite minimal improvement in epithelial disease, which aligns with the established understanding that rewetting provides primarily palliative benefits for epithelial pathology.

More specifically, transcriptomic analyses revealed an unexpected degree of keratocyte plasticity in response to prolonged desiccating stress and the transition of distressed keratocytes from a destructive to a reparative state following consistent, prolonged topical rewetting. This transition is associated with increased expression of extracellular matrix and BM components, along with reduced expression of matrix remodelers required for repair of both the stroma and BM. Our data further suggest that rewetting promotes this reparative shift, in part, by dampening proinflammatory MAPK signaling, which our analyses suggest is activated downstream of IL-1.

Upon ocular surface injury, keratocytes undergo well-described phenotypic changes, including early apoptosis of anterior stromal keratocytes and activation of surviving keratocytes into fibroblast-like cells that participate in stromal remodeling and wound repair, processes that collectively influence corneal transparency and stromal architecture.[12,76] The transition to an inflammatory phenotype occurs in numerous inflammatory diseases such as rheumatoid arthritis, inflammatory bowel disease (IBD), Sjogren's disease, and ulcerative colitis (UC).[77,78] This reprogramming is proposed as a two-step process, where exogenous inflammatory cytokines produced by immune cells trigger the transition of fibroblasts toward an inflammatory state which, in turn, produce high levels of inflammatory cytokines to amplify and sustain inflammation.[79] Consistent with this process, our study identifies a subset of inflammatory keratocytes in the desiccated cornea that highly express IL1b and co-express IL1R1, suggesting the potential activation of an IL-1 autocrine loop. Amplification of inflammation via an autocrine signaling loop has been shown in corneal fibroblasts grown *in vitro*[80] and is thought to impair wound healing. A similar mechanism has been reported in rheumatoid arthritis where a subset of synovial fibroblasts produce high levels of IL-6[81] through an autocrine loop involving leukocyte inhibitory factor (LIF) and its receptor, LIFR, resulting in the continuous production of inflammatory mediators that impair disease resolution.[82] Together, these studies suggest that targeting fibroblast cytokine signaling loops may represent a promising approach to attenuate fibroblast inflammatory responses and downstream tissue damage.

Consistent with this model of keratocyte activation, previous studies have demonstrated that keratocyte extracellular matrix gene expression is dynamically regulated during stromal injury and repair. In particular, inflammatory signaling and keratocyte activation have been reported to reduce expression of canonical keratocyte ECM genes including keratocan (Kera), lumican (Lum), and decorin (Dcn), especially as keratocytes transition toward fibroblast or myofibroblast phenotypes during corneal wound healing.[83–85] In our dataset, these same markers showed coordinated changes across keratocyte clusters under desiccating stress and following corneal rewetting, consistent with shifts in keratocyte transcriptional states rather than loss of keratocyte identity. These findings further support the concept that keratocytes are highly plastic stromal cells capable of dynamically adapting their ECM programs in response to inflammatory and reparative cues.

These transcriptional changes were mirrored at the structural level. Using TEM, we demonstrated extensive restoration of stromal architecture, including a significant improvement in collagen fibril organization and reduced interfibrillar distance, which is indicative of reduced stromal edema. This occurred alongside the notable downregulation of stromal *Col6* and upregulation of *Col4*, which are essential for rebuilding the BM.

While these data demonstrate the power of corneal rewetting on the stroma, it is important to emphasize that dry eye disease is a multifactorial condition characterized by alterations to the precorneal tear film quality and quantity, loss of corneal epithelial integrity, loss of corneal nerves, and infiltration of innate and adaptive immunecells. Rewetting the ocular surface improved stromal fiber organization and promoted BM repair in aqueous-deficient dry eye but it did not restore corneal innervation or epithelial barrier integrity. As a result, the therapeutic efficacy of corneal rewetting should be considered one part of a multifaceted treatment strategy targeting the diverse pathological mechanisms of dry eye disease, including epithelial repair, neuroregeneration, and immune modulation.

The clinical implications of these findings provide much-needed guidance to practicing clinicians with respect to how rewetting therapies benefit patients with aqueous-deficient dry eye. We provide clear evidence that corneal rewetting is an essential part of dry eye management and reveal a potential role for stromal fibroblast-targeted therapies as a previously unrecognized approach to restoring ocular surface health in dry eye. This is significant in that currently available FDA-approved anti-inflammatory agents have not proven to be sufficient to control the signs and symptoms of dry eye in most patients with moderate to severe cases. Furthermore, patients frequently report visual disturbances that cannot be corrected by refraction and the mechanistic basis for these symptoms have remained poorly understood.

Given that precise organization of the corneal stroma is essential for maintaining optical clarity, we postulate that rewetting with PBS may improve subjective vision through restoration of stromal architecture, even in the absence of significant epithelial improvement. This raises the possibility that over-the-counter rewetting drops, considered the clinical equivalent of PBS, have underappreciated therapeutic value for stromal health as well as visual function beyond their recognized palliative effects on surface comfort. Whether these findings extend to other models of dry eye remains to be determined, as stromal pathology has not been systematically examined across commonly used dry eye models. More broadly, these findings suggest that stromal keratocytes represent an active and therapeutically modifiable component of the ocular surface response to dry eye, rather than passive structural cells, and that targeting keratocyte state transitions may represent a previously underappreciated strategy for restoring corneal tissue homeostasis. Nevertheless, this work establishes a foundation for clinical investigations examining whether the restorative properties of corneal rewetting, in combination with anti-inflammatory and fibroblast-modulating therapies, can improve repair in dry eye disease. Such approaches may ultimately inform therapeutic strategies for restoring ocular surface homeostasis and reshape our future approach to dry eye management.

Limitations of the study

This study has several limitations. All findings are derived from a single mouse model of aqueous-deficient dry eye, and whether the stromal and keratocyte responses to rewetting generalize to other dry eye etiologies or models remains to be determined. The association between PBS treatment and attenuation of IL-1β-MAPK signaling is correlative, and direct causal relationships were not established. The study was conducted predominantly in female mice, reflecting the greater disease severity in female Aire KO animals, which limits generalizability to male disease phenotypes. Finally, functional validation of the inferred keratocyte subpopulation identities and signaling roles will be required to confirm the proposed reparative mechanisms.

RESOURCE AVAILABILITY

Lead contact

Further information and requests for resources and reagents should be directed to and will be fulfilled by the lead contact, Sarah M. Knox (sarah.knox@ucsf.edu).

Materials availability

This study did not generate new unique reagents.

Data and code availability

- RNA sequencing data have been deposited at the Gene Expression Omnibus (GEO) with accession code GSE272702 and are publicly available as the date of publication.
- Fiber orientation analysis code is shared in supplementary document.
- Any additional information required to reanalyze the data in this paper will be shared by the lead contact upon request.

ACKNOWLEDGMENTS

This work was supported by: National Eye Institute grants R01EY025980 (to S.M.K. and N.A.M.), R01EY027392 (to S.M.K.), and R01EY033040 (to S.M.K. and N.A.M.).

AUTHOR CONTRIBUTIONS

Conceptualization, Y.E., Y.T.C., L.A., N.A.M., and S.M.K.; methodology, Y.E., Y.T.C., L.A., S.V.N., D.P., K.N.C., M.A.R., N.A.M., and S.M.K.; investigation, Y.E., Y.T.C., L.A., S.V.N., K.N.C., D.P., M.A.R., N.A.M., and S.M.K.; data acquisition, Y.E., Y.T.C., L.A., K.N.C., D.P., S.V.N., M.A.R. and H.S.; visualization, Y.E., Y.T.C., S.V.N., L.A., and S.M.K.; funding acquisition, S.M.K. and

N.A.M.; project administration, S.M.K. and N.A.M.; supervision, S.M.K. and N.A.M.; writing – original draft, Y.E., Y.T.C., L.A., S.V.N., K.N.C., D.P., H.S., N.A.M., and S.M.K.; writing – review and editing, L.A., S.V.N., Y.T.C., M.A.R., N.A.M., and S.M.K.

DECLARATION OF INTERESTS

All authors declare no competing interests.

STAR★METHODS

Detailed methods are provided in the online version of this paper and include the following:

- KEY RESOURCES TABLE
- EXPERIMENTAL MODEL AND STUDY PARTICIPANT DETAILS
  - Animals
- METHOD DETAILS
  - Treatment regimen
  - *In situ* hybridization (RNAscope HiPlex) and quantification
  - Immunofluorescent analysis
  - Image quantification
  - Transmission electron microscopy (TEM) and quantification
  - RNA isolation and RNAseq library generation
  - Single-nucleus (sn) RNA-sequencing and analysis
- QUANTIFICATION AND STATISTICAL ANALYSIS

SUPPLEMENTAL INFORMATION

Supplemental information can be found online at https://doi.org/10.1016/j.isci.2026.116130.

Received: October 22, 2025
Revised: January 11, 2026
Accepted: May 12, 2026

REFERENCES

1. Donthineni, P.R., Doctor, M.B., Shanbhag, S., Kate, A., Galor, A., Djalilian, A.R., Singh, S., and Basu, S. (2023). Aqueous-deficient dry eye disease: Preferred practice pattern guidelines on clinical approach, diagnosis, and management. Indian J. Ophthalmol. *71*, 1332–1347. https://doi.org/10.4103/IJO.IJO_2808_22.
2. Mohamed, H.B., Abd El-Hamid, B.N., Fathalla, D., and Fouad, E.A. (2022). Current trends in pharmaceutical treatment of dry eye disease: A review. Eur. J. Pharmaceut. Sci. *175*, 106206. https://doi.org/10.1016/j.ejps.2022.106206.
3. Efraim, Y., Chen, F.Y.T., Cheong, K.N., Gaylord, E.A., McNamara, N.A., and Knox, S.M. (2022). A synthetic tear protein resolves dry eye through promoting corneal nerve regeneration. Cell Rep. *40*, 111307. https://doi.org/10.1016/j.celrep.2022.111307.
4. Hassell, J.R., and Birk, D.E. (2010). The molecular basis of corneal transparency. Exp. Eye Res. *91*, 326–335. https://doi.org/10.1016/j.exer.2010.06.021.
5. Espana, E.M., and Birk, D.E. (2020). Composition, structure and function of the corneal stroma. Exp. Eye Res. *198*, 108137. https://doi.org/10.1016/j.exer.2020.108137.
6. Meek, K.M. (2009). Corneal collagen-its role in maintaining corneal shape and transparency. Biophys. Rev. *1*, 83–93. https://doi.org/10.1007/s12551-009-0011-x.
7. Català, P., Groen, N., Dehnen, J.A., Soares, E., van Velthoven, A.J.H., Nuijts, R.M.M.A., Dickman, M.M., and LaPointe, V.L.S. (2021). Single cell transcriptomics reveals the heterogeneity of the human cornea to identify novel markers of the limbus and stroma. Sci. Rep. *11*, 21727. https://doi.org/10.1038/s41598-021-01015-w.
8. Iaccheri, B., Torroni, G., Cagini, C., Fiore, T., Cerquaglia, A., Lupidi, M., Cillino, S., and Dua, H.S. (2017). Corneal confocal scanning laser microscopy in patients with dry eye disease treated with topical cyclosporine. Eye *31*, 788–794. https://doi.org/10.1038/eye.2017.
9. Villani, E., Magnani, F., Viola, F., Santaniello, A., Scorza, R., Nucci, P., and Ratiglia, R. (2013). In vivo confocal evaluation of the ocular surface morpho-functional unit in dry eye. Optom. Vis. Sci. *90*, 576–586. https://doi.org/10.1097/OPX.0b013e318294c184.
10. Villani, E., Galimberti, D., Viola, F., Mapelli, C., and Ratiglia, R. (2007). The cornea in Sjogren's syndrome: an in vivo confocal study. Invest. Ophthalmol. Vis. Sci. *48*, 2017–2022. https://doi.org/10.1167/iovs.06-1129.
11. Villani, E., Garoli, E., Termine, V., Pichi, F., Ratiglia, R., and Nucci, P. (2015). Corneal Confocal Microscopy in Dry Eye Treated with Corticosteroids. Optom. Vis. Sci. *92*, e290–e295. https://doi.org/10.1097/OPX.0000000000000600.
12. West-Mays, J.A., and Dwivedi, D.J. (2006). The keratocyte: corneal stromal cell with variable repair phenotypes. Int. J. Biochem. Cell Biol. *38*, 1625–1631. https://doi.org/10.1016/j.biocel.2006.03.010.
13. Efraim, Y., Chen, F.Y.T., Stashko, C., Cheong, K.N., Gaylord, E., McNamara, N., and Knox, S.M. (2020). Alterations in corneal biomechanics underlie early stages of autoimmune-mediated dry eye disease. J. Autoimmun. *114*, 102500. https://doi.org/10.1016/j.jaut.2020.102500.
14. Tsubota, K. (1998). Tear dynamics and dry eye. Prog. Retin. Eye Res. *17*, 565–596.
15. Zhou, D., Chen, Y.-T., Chen, F., Gallup, M., Vijmasi, T., Bahrami, A.F., Noble, L.B., van Rooijen, N., and McNamara, N.A. (2012). Critical involvement of macrophage infiltration in the development of Sjögren's syndrome-associated dry eye. Am. J. Pathol. *181*, 753–760. https://doi.org/10.1016/j.ajpath.2012.05.014.
16. Chen, F.Y., Lee, A., Ge, S., Nathan, S., Knox, S.M., and McNamara, N.A. (2017). Aire-deficient mice provide a model of corneal and lacrimal gland neuropathy in Sjögren's syndrome. PLoS One *12*, e0184916. https://doi.org/10.1371/journal.pone.0184916.
17. Meek, K.M., and Knupp, C. (2015). Corneal structure and transparency. Prog. Retin. Eye Res. *49*, 1–16. https://doi.org/10.1016/j.preteyeres.2015.07.001.
18. Espana, E.M., Kawakita, T., Di Pascuale, M.A., Li, W., Yeh, L.K., Parel, J.M., Liu, C.Y., and Tseng, S.C.G. (2005). The heterogeneous murine corneal stromal cell populations in vitro. Invest. Ophthalmol. Vis. Sci. *46*, 4528–4535. https://doi.org/10.1167/iovs.05-0117.
19. Chen, S., Oldberg, A., Chakravarti, S., and Birk, D.E. (2010). Fibromodulin regulates collagen fibrillogenesis during peripheral corneal development. Dev. Dyn. *239*, 844–854. https://doi.org/10.1002/dvdy.22216.
20. Zheng, Z., James, A.W., Li, C., Jiang, W., Wang, J.Z., Chang, G.X., Lee, K.S., Chen, F., Berthiaume, E.A., Chen, Y., et al. (2017). Fibromodulin reduces scar formation in adult cutaneous wounds by eliciting a fetal-like phenotype. Signal Transduct. Targeted Ther. *2*, 17050. https://doi.org/10.1038/sigtrans.2017.50.
21. Cooper, J.G., Jeong, S.J., McGuire, T.L., Sharma, S., Wang, W., Bhattacharyya, S., Varga, J., and Kessler, J.A. (2018). Fibronectin EDA forms the chronic fibrotic scar after contusive spinal cord injury. Neurobiol. Dis. *116*, 60–68. https://doi.org/10.1016/j.nbd.2018.04.014.
22. Walker, J.T., McLeod, K., Kim, S., Conway, S.J., and Hamilton, D.W. (2016). Periostin as a multifunctional modulator of the wound healing response. Cell Tissue Res. *365*, 453–465. https://doi.org/10.1007/s00441-016-2426-6.
23. Nerusu, K.C., Warner, R.L., Bhagavathula, N., McClintock, S.D., Johnson, K.J., and Varani, J. (2007). Matrix metalloproteinase-3 (stromelysin-1) in acute inflammatory tissue injury. Exp. Mol. Pathol. *83*, 169–176. https://doi.org/10.1016/j.yexmp.2007.04.003.

24. Kim, D.J., Christofidou, E.D., Keene, D.R., Hassan Milde, M., and Adams, J.C. (2015). Intermolecular interactions of thrombospondins drive their accumulation in extracellular matrix. Mol. Biol. Cell *26*, 2640–2654. https://doi.org/10.1091/mbc.E14-05-0996.

25. Kyriakides, T.R., and Maclauchlan, S. (2009). The role of thrombospondins in wound healing, ischemia, and the foreign body reaction. J. Cell Commun. Signal. *3*, 215–225. https://doi.org/10.1007/s12079-009-0077-z.

26. Bardag-Gorce, F., Hoffman, C., Meepe, I., Ferrini, M., Hoft, R.H., Oliva, J., and Niihara, Y. (2023). Thrombospondin-1 induction and VEGF reduction by proteasome inhibition. Heliyon *9*, e13397. https://doi.org/10.1016/j.heliyon.2023.e13397.

27. Franzke, C.-W., Bruckner, P., and Bruckner-Tuderman, L. (2005). Collagenous transmembrane proteins: recent insights into biology and pathology. J. Biol. Chem. *280*, 4005–4008. https://doi.org/10.1074/jbc.R400034200.

28. Spivey, K.A., Chung, I., Banyard, J., Adini, I., Feldman, H.A., and Zetter, B.R. (2012). A role for collagen XXIII in cancer cell adhesion, anchorage-independence and metastasis. Oncogene *31*, 2362–2372. https://doi.org/10.1038/onc.2011.406.

29. Woronkowicz, M., Roberts, H., and Skopiński, P. (2024). The Role of Insulin-like Growth Factor (IGF) System in the Corneal Epithelium Homeostasis-From Limbal Epithelial Stem Cells to Therapeutic Applications. Biology (Basel). *13*, 144. https://doi.org/10.3390/biology13030144.

30. Trosan, P., Javorkova, E., Zajicova, A., Hajkova, M., Hermankova, B., Kossl, J., Krulova, M., and Holan, V. (2016). The Supportive Role of Insulin-Like Growth Factor-I in the Differentiation of Murine Mesenchymal Stem Cells into Corneal-Like Cells. Stem Cell. Dev. *25*, 874–881. https://doi.org/10.1089/scd.2016.0030.

31. Himburg, H.A., Termini, C.M., Schlussel, L., Kan, J., Li, M., Zhao, L., Fang, T., Sasine, J.P., Chang, V.Y., and Chute, J.P. (2018). Distinct bone marrow sources of pleiotrophin control hematopoietic stem cell maintenance and regeneration. Cell Stem Cell *23*, 370–381.e5. https://doi.org/10.1016/j.stem.2018.07.003.

32. Sumioka, T., Iwanishi, H., Okada, Y., Nidegawa, Y., Miyajima, M., Matsumoto, K., and Saika, S. (2018). Loss of tenascin X gene function impairs injury-induced stromal angiogenesis in mouse corneas. J. Cell. Mol. Med. *22*, 948–956. https://doi.org/10.1111/jcmm.13397.

33. Sumioka, T., Iwanishi, H., Okada, Y., Miyajima, M., Ichikawa, K., Reinach, P.S., Matsumoto, K.i., and Saika, S. (2021). Impairment of corneal epithelial wound healing is association with increased neutrophil infiltration and reactive oxygen species activation in tenascin X-deficient mice. Lab. Invest. *101*, 690–700. https://doi.org/10.1038/s41374-021-00576-8.

34. Jollymore, A., Lethias, C., Peng, Q., Cao, Y., and Li, H. (2009). Nanomechanical properties of tenascin-X revealed by single-molecule force spectroscopy. J. Mol. Biol. *385*, 1277–1286. https://doi.org/10.1016/j.jmb.2008.11.038.

35. Margaron, Y., Bostan, L., Exposito, J.-Y., Malbouyres, M., Trunfio-Sfarghiu, A.M., Berthier, Y., and Lethias, C. (2010). Tenascin-X increases the stiffness of collagen gels without affecting fibrillogenesis. Biophys. Chem. *147*, 87–91. https://doi.org/10.1016/j.bpc.2009.12.011.

36. Egging, D., van den Berkmortel, F., Taylor, G., Bristow, J., and Schalkwijk, J. (2007). Interactions of human tenascin-X domains with dermal extracellular matrix molecules. Arch. Dermatol. Res. *298*, 389–396. https://doi.org/10.1007/s00403-006-0706-9.

37. Minamitani, T., Ikuta, T., Saito, Y., Takebe, G., Sato, M., Sawa, H., Nishimura, T., Nakamura, F., Takahashi, K., Ariga, H., and Matsumoto, K.i. (2004). Modulation of collagen fibrillogenesis by tenascin-X and type VI collagen. Exp. Cell Res. *298*, 305–315. https://doi.org/10.1016/j.yexcr.2004.04.030.

38. Egging, D.F., van Vlijmen, I., Starcher, B., Gijsen, Y., Zweers, M.C., Blankevoort, L., Bristow, J., and Schalkwijk, J. (2006). Dermal connective tissue development in mice: an essential role for tenascin-X. Cell Tissue Res. *323*, 465–474. https://doi.org/10.1007/s00441-005-0100-5.

39. Buechler, M.B., Pradhan, R.N., Krishnamurty, A.T., Cox, C., Calviello, A.K., Wang, A.W., Yang, Y.A., Tam, L., Caothien, R., Roose-Girma, M., et al. (2021). Cross-tissue organization of the fibroblast lineage. Nature *593*, 575–579. https://doi.org/10.1038/s41586-021-03549-5.

40. Jin, S., Plikus, M.V., and Nie, Q. (2025). CellChat for systematic analysis of cell-cell communication from single-cell transcriptomics. Nat. Protoc. *20*, 180–219. https://doi.org/10.1038/s41596-024-01045-4.

41. Theocharidis, G., Drymoussi, Z., Kao, A.P., Barber, A.H., Lee, D.A., Braun, K.M., and Connelly, J.T. (2016). Type VI collagen regulates dermal matrix assembly and fibroblast motility. J. Invest. Dermatol. *136*, 74–83. https://doi.org/10.1038/JID.2015.352.

42. Mereness, J.A., Bhattacharya, S., Wang, Q., Ren, Y., Pryhuber, G.S., and Mariani, T.J. (2018). Type VI collagen promotes lung epithelial cell spreading and wound-closure. PLoS One *13*, e0209095. https://doi.org/10.1371/journal.pone.0209095.

43. Williams, L.M., McCann, F.E., Cabrita, M.A., Layton, T., Cribbs, A., Knezevic, B., Fang, H., Knight, J., Zhang, M., Fischer, R., et al. (2020). Identifying collagen VI as a target of fibrotic diseases regulated by CREBBP/EP300. Proc Natl Acad Sci USA *117*, 20753–20763. https://doi.org/10.1073/pnas.2004281117.

44. Uno, K., Hayashi, H., Kuroki, M., Uchida, H., Yamauchi, Y., Kuroki, M., and Oshima, K. (2004). Thrombospondin-1 accelerates wound healing of corneal epithelia. Biochem. Biophys. Res. Commun. *315*, 928–934. https://doi.org/10.1016/j.bbrc.2004.01.146.

45. Zhao, C., Li, W., Duan, H., Li, Z., Jia, Y., Zhang, S., Wang, X., Zhou, Q., and Shi, W. (2020). NAD+ precursors protect corneal endothelial cells from UVB-induced apoptosis. Am. J. Physiol. Cell Physiol. *318*, C796–C805. https://doi.org/10.1152/ajpcell.00445.2019.

46. Tokunaga, R., Zhang, W., Naseem, M., Puccini, A., Berger, M.D., Soni, S., McSkane, M., Baba, H., and Lenz, H.J. (2018). CXCL9, CXCL10, CXCL11/CXCR3 axis for immune activation - A target for novel cancer therapy. Cancer Treat. Rev. *63*, 40–47. https://doi.org/10.1016/j.ctrv.2017.11.007.

47. Sidney, L.E., Branch, M.J., Dunphy, S.E., Dua, H.S., and Hopkinson, A. (2014). Concise review: evidence for CD34 as a common marker for diverse progenitors. Stem Cell. *32*, 1380–1389. https://doi.org/10.1002/stem.1661.

48. Stzepourginski, I., Nigro, G., Jacob, J.-M., Dulauroy, S., Sansonetti, P.J., Eberl, G., and Peduto, L. (2017). CD34+ mesenchymal cells are a major component of the intestinal stem cells niche at homeostasis and after injury. Proc Natl Acad Sci USA *114*, E506–E513. https://doi.org/10.1073/pnas.1620059114.

49. Joseph, A., Hossain, P., Jham, S., Jones, R.E., Tighe, P., McIntosh, R.S., and Dua, H.S. (2003). Expression of CD34 and L-selectin on human corneal keratocytes. Invest. Ophthalmol. Vis. Sci. *44*, 4689–4692. https://doi.org/10.1167/iovs.02-0999.

50. Lin, J.B., Shen, X., Pfeifer, C.W., Shiau, F., Santeford, A., Ruzycki, P.A., Clark, B.S., Liu, Q., Huang, A.J.W., and Apte, R.S. (2023). Dry eye disease in mice activates adaptive corneal epithelial regeneration distinct from constitutive renewal in homeostasis. Proc Natl Acad Sci USA *120*, e2204134120. https://doi.org/10.1073/pnas.2204134120.

51. Chlenski, A., and Cohn, S.L. (2010). Modulation of matrix remodeling by SPARC in neoplastic progression. Semin. Cell Dev. Biol. *21*, 55–65. https://doi.org/10.1016/j.semcdb.2009.11.018.

52. Seong, H., Song, C., Kim, M., Yoo, W.S., Choi, M.Y., Varga, R.D., Choe, Y.H., Lee, B., Yun, S.P., Yoo, Y.S., et al. (2026). Periostin deletion reduces corneal opacity and the infiltration of immune cells. Am. J. Pathol. *196*, 550–561. https://doi.org/10.1016/j.ajpath.2025.09.007.

53. Persson, T., Monsef, N., Andersson, P., Bjartell, A., Malm, J., Calafat, J., and Egesten, A. (2003). Expression of the neutrophil-activating CXC chemokine ENA-78/CXCL5 by human eosinophils. Clin. Exp. Allergy *33*, 531–537. https://doi.org/10.1046/j.1365-2222.2003.01609.x.

54. Li, W., Wang, W., Zuo, R., Liu, C., Shu, Q., Ying, H., and Sun, K. (2017). Induction of pro-inflammatory genes by serum amyloid A1 in human amnion

fibroblasts. Sci. Rep. *7*, 693. https://doi.org/10.1038/s41598-017-00782-9.

55. Vieira, S.M., Lemos, H.P., Grespan, R., Napimoga, M., Dal-Secco, D., Freitas, A., Cunha, T., Verri Jr, W., Souza-Junior, D., Jamur, M., et al. (2009). A crucial role for TNF-alpha in mediating neutrophil influx induced by endogenously generated or exogenous chemokines, KC/CXCL1 and LIX/CXCL5. Br. J. Pharmacol. *158*, 779–789. https://doi.org/10.1111/j.1476-5381.2009.00367.x.
56. Königshoff, M., Wilhelm, A., Jahn, A., Sedding, D., Amarie, O.V., Eul, B., Seeger, W., Fink, L., Günther, A., Eickelberg, O., and Rose, F. (2007). The angiotensin II receptor 2 is expressed and mediates angiotensin II signaling in lung fibrosis. Am. J. Respir. Cell Mol. Biol. *37*, 640–650. https://doi.org/10.1165/rcmb.2006-0379TR.
57. De Buck, M., Gouwy, M., Wang, J.M., Van Snick, J., Proost, P., Struyf, S., and Van Damme, J. (2016). The cytokine-serum amyloid A-chemokine network. Cytokine Growth Factor Rev. *30*, 55–69. https://doi.org/10.1016/j.cytogfr.2015.12.010.
58. Guerrero-Juarez, C.F., Dedhia, P.H., Jin, S., Ruiz-Vega, R., Ma, D., Liu, Y., Yamaga, K., Shestova, O., Gay, D.L., Yang, Z., et al. (2019). Single-cell analysis reveals fibroblast heterogeneity and myeloid-derived adipocyte progenitors in murine skin wounds. Nat. Commun. *10*, 650. https://doi.org/10.1038/s41467-018-08247-x.
59. Chen, X., Liu, Q., Huang, W., Cai, C., Xia, W., Peng, Y., Zheng, S., Li, G., Xu, Y., Wang, J., et al. (2018). Stanniocalcin-2 contributes to mesenchymal stromal cells attenuating murine contact hypersensitivity mainly via reducing CD8+ Tc1 cells. Cell Death Dis. *9*, 548. https://doi.org/10.1038/s41419-018-0614-x.
60. Wilson, S.E. (2022). The yin and yang of mesenchymal cells in the corneal stromal fibrosis response to injury: the cornea as a model of fibrosis in other organs. Biomolecules *13*, 87. https://doi.org/10.3390/biom13010087.
61. Jordan, A.R., Racine, R.R., Hennig, M.J.P., and Lokeshwar, V.B. (2015). The role of CD44 in disease pathophysiology and targeted treatment. Front. Immunol. *6*, 182. https://doi.org/10.3389/fimmu.2015.00182.
62. Shi, X., Leng, L., Wang, T., Wang, W., Du, X., Li, J., McDonald, C., Chen, Z., Murphy, J.W., Lolis, E., et al. (2006). CD44 is the signaling component of the macrophage migration inhibitory factor-CD74 receptor complex. Immunity *25*, 595–606. https://doi.org/10.1016/j.immuni.2006.08.020.
63. Voss, S., Krüger, S., and Scherschel, K. (2019). Macrophage Migration Inhibitory Factor (MIF) Expression Increases during Myocardial Infarction and Supports Pro-Inflammatory Signaling in Cardiac Fibroblasts. Biomolecules *9*, 38. https://doi.org/10.3390/biom9020038.
64. Honda, A., Abe, R., Makino, T., Norisugi, O., Fujita, Y., Watanabe, H., Nishihira, J., Iwakura, Y., Yamagishi, S.i., Shimizu, H., and Shimizu, T. (2008). Interleukin-1beta and macrophage migration inhibitory factor (MIF) in dermal fibroblasts mediate UVA-induced matrix metalloproteinase-1 expression. J. Dermatol. Sci. *49*, 63–72. https://doi.org/10.1016/j.jdermsci.2007.09.007.
65. West-Mays, J.A., Sadow, P.M., Tobin, T.W., Strissel, K.J., Cintron, C., and Fini, M.E. (1997). Repair phenotype in corneal fibroblasts is controlled by an interleukin-1 alpha autocrine feedback loop. Invest Ophthalmol Vis Sci. *38*, 1367–1379.
66. Girard, M.T., Matsubara, M., and Fini, M.E. (1991). Transforming growth factor-beta and interleukin-1 modulate metalloproteinase expression by corneal stromal cells. Invest Ophthalmol Vis. Sci. *32*, 2441–2454.
67. Broderick, L., and Hoffman, H.M. (2022). IL-1 and autoinflammatory disease: biology, pathogenesis and therapeutic targeting. Nat. Rev. Rheumatol. *18*, 448–463. https://doi.org/10.1038/s41584-022-00797-1.
68. Wilson, S.E., and Esposito, A. (2009). Focus on molecules: interleukin-1: a master regulator of the corneal response to injury. Exp. Eye Res. *89*, 124–125. https://doi.org/10.1016/j.exer.2009.02.011.
69. Kolb, M., Margetts, P.J., Anthony, D.C., Pitossi, F., and Gauldie, J. (2001). Transient expression of IL-1beta induces acute lung injury and chronic repair leading to pulmonary fibrosis. J. Clin. Investig. *107*, 1529–1536. https://doi.org/10.1172/JCI12568.
70. Chen, Y.-T., Lazarev, S., Bahrami, A.F., Noble, L.B., Chen, F.Y.T., Zhou, D., Gallup, M., Yadav, M., and McNamara, N.A. (2012). Interleukin-1 receptor mediates the interplay between CD4+ T cells and ocular resident cells to promote keratinizing squamous metaplasia in Sjögren's syndrome. Lab. Invest. *92*, 556–570. https://doi.org/10.1038/labinvest.2011.189.
71. Luo, L., Li, D.-Q., Doshi, A., Farley, W., Corrales, R.M., and Pflugfelder, S.C. (2004). Experimental dry eye stimulates production of inflammatory cytokines and MMP-9 and activates MAPK signaling pathways on the ocular surface. Invest. Ophthalmol. Vis. Sci. *45*, 4293–4301. https://doi.org/10.1167/iovs.03-1145.
72. Wan, X., Cheng, M., Xin, C., Lu, Y., Yang, P., Zhou, S., Zhou, X., Le, Q., Sun, J., Zhou, F., et al. (2025). Identification of matrix metalloproteinase 3 as a potential biomarker for dry eye disease. Transl. Vis. Sci. Technol. *14*, 23. https://doi.org/10.1167/tvst.14.7.23.
73. Wilson, S.E., Torricelli, A.A.M., and Marino, G.K. (2020). Corneal epithelial basement membrane: Structure, function and regeneration. Exp. Eye Res. *194*, 108002. https://doi.org/10.1016/j.exer.2020.108002.
74. Hohenester, E., and Yurchenco, P.D. (2013). Laminins in basement membrane assembly. Cell Adhes. Migrat. *7*, 56–63. https://doi.org/10.4161/cam.21831.
75. Morales, S.A., Mareninov, S., Coulam, P., Wadehra, M., Goodglick, L., Braun, J., and Gordon, L.K. (2009). Functional consequences of interactions between FAK and epithelial membrane protein 2 (EMP2). Invest. Ophthalmol. Vis. Sci. *50*, 4949–4956. https://doi.org/10.1167/iovs.08-3315.
76. Wilson, S.E., Mohan, R.R., Mohan, R.R., Ambrósio, R., Hong, J., and Lee, J. (2001). The corneal wound healing response. Prog. Retin. Eye Res. *20*, 625–637. https://doi.org/10.1016/S1350-9462(01)00008-8.
77. Mizoguchi, F., Slowikowski, K., Wei, K., Marshall, J.L., Rao, D.A., Chang, S.K., Nguyen, H.N., Noss, E.H., Turner, J.D., Earp, B.E., et al. (2018). Functionally distinct disease-associated fibroblast subsets in rheumatoid arthritis. Nat. Commun. *9*, 789. https://doi.org/10.1038/s41467-018-02892-y.
78. Cadinu, P., Sivanathan, K.N., Misra, A., Xu, R.J., Mangani, D., Yang, E., Rone, J.M., Tooley, K., Kye, Y.C., Bod, L., et al. (2024). Charting the cellular biogeography in colitis reveals fibroblast trajectories and coordinated spatial remodeling. Cell *187*, 2010–2028.e30. https://doi.org/10.1016/j.cell.2024.03.013.
79. Wei, K., Nguyen, H.N., and Brenner, M.B. (2021). Fibroblast pathology in inflammatory diseases. J. Clin. Investig. *131*, e149538. https://doi.org/10.1172/JCI149538.
80. West-Mays, J.A., Strissel, K.J., Sadow, P.M., and Fini, M.E. (1995). Competence for collagenase gene expression by tissue fibroblasts requires activation of an interleukin 1 alpha autocrine loop. Proc Natl Acad Sci USA *92*, 6768–6772. https://doi.org/10.1073/pnas.92.15.6768.
81. Zhang, F., Wei, K., Slowikowski, K., Fonseka, C.Y., Rao, D.A., Kelly, S., Goodman, S.M., Tabechian, D., Hughes, L.B., Salomon-Escoto, K., et al. (2019). Defining inflammatory cell states in rheumatoid arthritis joint synovial tissues by integrating single-cell transcriptomics and mass cytometry. Nat. Immunol. *20*, 928–942. https://doi.org/10.1038/s41590-019-0378-1.
82. Nguyen, H.N., Noss, E.H., Mizoguchi, F., Huppertz, C., Wei, K.S., Watts, G.F., and Brenner, M.B. (2017). Autocrine Loop Involving IL-6 Family Member LIF, LIF Receptor, and STAT4 Drives Sustained Fibroblast Production of Inflammatory Mediators. Immunity *46*, 220–232. https://doi.org/10.1016/j.immuni.2017.01.004.
83. de Preux, M., Klopfenstein Bregger, M.D., Brünisholz, H.P., Van der Vekens, E., Schweizer-Gorgas, D., and Koch, C. (2020). Clinical use of computer-assisted orthopedic surgery in horses. Vet. Surg. *49*, 1075–1087. https://doi.org/10.1111/vsu.13486.

84. Funderburgh, J.L., Funderburgh, M.L., Mann, M.M., Corpuz, L., and Roth, M.R. (2001). Proteoglycan expression during transforming growth factor beta -induced keratocyte-myofibroblast transdifferentiation. J. Biol. Chem. *276*, 44173–44178. https://doi.org/10.1074/jbc.M107596200.

85. Funderburgh, J.L., Mann, M.M., and Funderburgh, M.L. (2003). Keratocyte phenotype mediates proteoglycan structure: a role for fibroblasts in corneal fibrosis. J. Biol. Chem. *278*, 45629–45637. https://doi.org/10.1074/jbc.M303292200.

86. Liu, Y., Keikhosravi, A., Mehta, G.S., Drifka, C.R., and Eliceiri, K.W. (2017). Methods for quantifying fibrillar collagen alignment. Methods Mol. Biol. *1627*, 429–451. https://doi.org/10.1007/978-1-4939-7113-8_28.

87. Chen, S., Zhou, Y., Chen, Y., and Gu, J. (2018). fastp: an ultra-fast all-in-one FASTQ preprocessor. Bioinformatics *34*, i884–i890. https://doi.org/10.1093/bioinformatics/bty560.

88. Dobin, A., Davis, C.A., Schlesinger, F., Drenkow, J., Zaleski, C., Jha, S., Batut, P., Chaisson, M., and Gingeras, T.R. (2013). STAR: ultrafast universal RNA-seq aligner. Bioinformatics *29*, 15–21. https://doi.org/10.1093/bioinformatics/bts635.

89. Love, M.I., Huber, W., and Anders, S. (2014). Moderated estimation of fold change and dispersion for RNA-seq data with DESeq2. Genome Biol. *15*, 550. https://doi.org/10.1186/s13059-014-0550-8.

90. Aibar, S., González-Blas, C.B., Moerman, T., Huynh-Thu, V.A., Imrichova, H., Hulselmans, G., Rambow, F., Marine, J.C., Geurts, P., Aerts, J., et al. (2017). SCENIC: single-cell regulatory network inference and clustering. Nat. Methods *14*, 1083–1086. https://doi.org/10.1038/nmeth.4463.

91. Huynh-Thu, V.A., Irrthum, A., Wehenkel, L., and Geurts, P. (2010). Inferring regulatory networks from expression data using tree-based methods. PLoS One *5*, e12776. https://doi.org/10.1371/journal.pone.0012776.

STAR★METHODS

KEY RESOURCES TABLE

REAGENT or RESOURCE	SOURCE	IDENTIFIER
Antibodies		
rabbit anti-LAMA3	Abcam	Cat 151715
rat anti-Perlecan	Chemicon	MAB1948
Rabbit anti-COL1	Abcam	Cat 34710; RRID: AB_731684
rabbit anti-CD34	Abcam	Cat. ab81289; RRID: AB_1640331
mouse anti-pMAK	Upstate	Cat. 05-481
rabbit anti-pFAK	Abcam	Cat.223529; RRID: AB_1267144
rabbit anti-IL1R1	Santa Cruz	Cat. sc-689; RRID: AB_631807
goat anti-IL1b	R&D	Cat. AF-401_NA; RRID: AB_416684
Chemicals, peptides, and recombinant proteins		
Dulbeccos' Phosphate-Buffered Saline (DPBS)	CORNING	21-031-CM
16% paraformaldehyde	ThermoFisher	043368.9M
RNAscope® Protease IV	ACDBio	322336
RNAscope Probe: Mm-Mmp3	ACDBio	480961
RNAscope Probe: Mm-Fmod	ACDBio	479421
RNAscope Probe: Mm-Col6a1	ACDBio	443261
RNAscope Probe: Mm-Nampt	ACDBio	577461
RNAscope Probe: Mm-Cxcl9	ACDBio	489341
RNAscope Probe: Mm-Col1a1	ACDBio	319371
RNAscope Probe: Mm-Col6a1	ACDBio	443261
RNAscope Probe: Mm-Thbs1	ACDBio	443261
DAPI	ACDBio	324420
70% ethanol	Sigma	E7023
Acetone	Sigma	179124
Epon resin	Electron Microscopy Sciences	14121
Uranyl Acetate	Ted Pella Inc	19481
Osmium tetroxide	Ted Pella Inc	18451
Lead citrate Reynolds stain	ThermoFisher	50-209-0574
Hoechst	Sigma-Aldrich	T5840
Critical commercial assays		
RNAscope™ HiPlex Assay v2	ACDBio	324440
Chromium snRNA sequencing	10x Genomics	GEM-X
Deposited data		
RNA sequencing data	Gene expression Omnibus	GSE272702
Experimental models: Organisms/strains		
Mouse: Aire-deficient	UCSF in house: Dr. Mark Anderson	https://doi.org/10.1126/science.1075958
Mouse: Balb/C	The Jackson Laboratory	RRID:IMSR_JAX:000651
Software and algorithms		
Fiji/ImageJ	Distribution of ImageJ	https://imagej.net/software/fiji/downloads
ZEN	Zeiss	https://www.zeiss.com/microscopy/us/products/software/zeiss-zen.html
Seurat (v5.0.0)	Satijalab	https://satijalab.org/seurat/
R	The R Project	https://www.r-project.org/
GraphPad Prism	GraphPad Software Inc	RRID:SCR_002798; https://www.graphpad.com

(*Continued on next page*)

Continued

REAGENT or RESOURCE	SOURCE	IDENTIFIER
CurveAlign-CT-FIRE	Laboratory for Optical and Computational Instrumentation	CurveAlign (https://loci.wisc.edu/curvealign/), CT-Fire (https://loci.wisc.edu/ctfire/)
MATLAB	Mathworks	https://www.mathworks.com/products/matlab.html
Digital Micrograph 3	Gatan Inc., Pleasanton, CA	https://www.gatan.com/products/tem-analysis/digitalmicrograph-software

EXPERIMENTAL MODEL AND STUDY PARTICIPANT DETAILS

Animals

All procedures were approved by the UCSF Institutional Animal Care and Use Committee (IACUC, Protocol: AN203203). Wild type (WT) and *Aire*-deficient mice on the BALB/c background (BALB/c *Aire* KO) were the gift of Mark Anderson, University of California, San Francisco. Mice were housed under specific pathogen-free conditions at 22°C with a 12-h light/dark cycle and *ad libitum* access to food and water. Adult female mice (aged 5–7 weeks) were used in all experiments as male mice do not reliably develop the aqueous-deficient phenotype required for this experimental model; this is acknowledged as a limitation.

METHOD DETAILS

Treatment regimen

Aire KO mice (5+) were topically treated with 5μL/eye of PBS 3x daily for 14 consecutive days. Corneas were harvested after 24hrs and processed for global RNAseq. After 14 days corneas were collected for *in situ*/immunofluorescence analysis, and snRNAseq.

In situ hybridization (RNAscope HiPlex) and quantification

RNAscope™ HiPlex Assay v2 (ACDBio) was performed on 5–8 mice using company protocols on fresh frozen cornea tissue sections to detect target RNA at single cell level. Tissue pre-treatment included fixation for 60 min in 4% paraformaldehyde (PFA) at RT, Dehydrate the sections in 50%, 70%, and 100% ethanol followed by protease IV treatment (RNAscope® Protease IV ACD# 322336) for 30 min at RT. Target probes were hybridized for 2 h at 40°C using the HybEZ Oven followed by amplification steps according to the manufacturer's protocol. Briefly, treatment with Amp 1 (ACDBio Cat. 324111), Amp 2 (ACDBio, Cat. 324112), and Amp 3 (ACDBio, Cat. 324113) were performed for 30 min each at 40°C. Mouse Positive Control Probe (ACD Probe: 320881) and Negative Control Probe (ACD Probe: 320871) were included in the assay. Detection of specific probe binding sites was with RNAscope HiPlex12 Detection Reagents (488, 550, 650) kit v2 (ACDBio, Cat. 324410). Detection of the first 3 probes were with Fluoro T1-T3 (Cat. 324411) for 15 min at 40°C and counterstained with DAPI (Cat. 324420). Positive staining was indicated by fluorescent dots in the cell cytoplasm or nucleus. Slides were mounted and imaged at 40x magnification on a Zeiss Yokogawa Spinning disk confocal microscope. Fluorophores T4-T6 (Cat. 324412), T7-T9 (Cat. 324413), and T10-T12 (Cat. 324414) were added in subsequent rounds. To remove the coverslips, slides were soaked in 4X SSC and the fluorophore was removed using a 10% cleaving solution (Cat. 324130) incubated for 15 min at RT twice.

Image analysis was performed utilizing Qupath, a bioimage analysis software. Images taken at 40x magnification were uploaded and regions of interest were drawn to include sections of the corneal stroma at the limbus and central cornea. ROIs were 200 μm in length for the limbus, 350 μm in length for the central cornea, and 500 μm for the limbal peripheral cornea, and included the entire area between the corneal endothelium and epithelial BM. Analysis of the limbal peripheral cornea was performed at the 2 sites per tissue section. Qupath's cell detection feature was used to quantify nuclei staining and subcellular detection was used to quantify the number of RNA puncta within the cell. The threshold intensity for nuclei detection was set to 10, and cell expansion was set at 5 μm from the detected nuclei. Thresholds for subcellular spot detection were determined using negative control images. Threshold values that yielding 10% or less of total detections on the negative control were applied to the target images. Thresholds for fluorophore levels per cell were set at >50 for high and <20 for low expression.

Immunofluorescent analysis

Samples were analyzed via immunofluorescence as previously described.[13] Briefly, enucleated eyes were embedded in OCT Tissue Tek freezing media. Sections of 7 μm and 20 μm were prepared from fresh frozen tissues using a cryostat (Leica, Izar, Germany) and mounted on SuperFrost Plus slides. Sections were fixed for 20 min in 4% paraformaldehyde (PFA) at room temperature (RT), permeabilized with 0.3% Triton X-100 in phosphate buffered saline for 15 min, washed in PBS-Tween 20 (PBST) for 10 min, and blocked with 5% normal donkey serum (Jackson Laboratories, ME) in PBST for 1 h at RT. Slides were incubated with primary antibodies diluted in blocking buffer overnight at 4°C. Primary antibodies used: rabbit anti-LAMA3 (1:500, Abcam, Cat 151715), rat anti-Perlecan (HSPG2) (1:500 Chemicon, MAB1948), rabbit anti-COL1(1:500, Abcam, Cat 34710), rabbit anti-CD34 (1:500, Abcam, Cat. ab81289), mouse anti-pMAK (1:200, Upstate, Cat. 05–481), rabbit anti-pFAK (1:500, Abcam, Cat.223529), rabbit anti-IL1R1 (1:400, Santa Cruz,

Cat. sc-689), goat anti-IL1b (1:20, R&D, Cat. AF-401_NA). Following 3 washes with PBST, antibodies were detected using Cy2-, Cy3- or Cy5-conjugated secondary Fab fragment antibodies (Jackson Laboratories), and nuclei were stained with Hoechst 33342 (1:3000, Sigma-Aldrich). Tissue sections were imaged using a Zeiss LSM 900 confocal microscope or Zeiss Yokogawa Spinning disk confocal microscope with images assessed using NIH ImageJ software,[73] as described below.

Image quantification

Basement membrane (BM) and extracellular matrix (ECM)

Laminin (LAM) and perlecan (HSPG2) intensities were quantified on 300 μm sections of central corneal BM ROI applying Tsai's thresholding method (Moments) (ref), integrated densities within the ROI of the thresholded image were recorded. Alignment of collagen I fibers and fiber thickness were measured using CurveAlign CT-FIRE mode according to software protocol[74] and the angle of each extracted fiber was calculated and recorded by the software. Frequency distribution histograms of the different groups were created using PRISM (n>=5) and subjected to Gaussian curve fit (Figure S1A).

Mechanosensor pFAK

pFAK fluorescent intensity was quantified on a ROI containing a 350 μm section of central cornea epithelial BM. Tsai's thresholding method (Moments) was applied to the ROI of each cornea, and integrated densities within the ROI of the thresholded image were recorded.

pMAK and Il1b

pMAK activity level was quantified on a ROI containing the stromal area under 350 μm section of central cornea epithelial BM. Tsai's thresholding method (moments) was applied to the ROI of each cornea, and percent area of threshold signal within the ROI of the thresholded image were recorded. *Il1b* high keratocytes were identified visually and manually counted within 1000um of cornea cross-section. To exclude immune cells that also expressed *Il1b*, only $Il1b^{high}Il1r1^{+}$ cells were counted immune cells in the cornea do not express IL1R1

Transmission electron microscopy (TEM) and quantification

Corneal stroma tissues were fixed in 2% glutaraldehyde and 2% paraformaldehyde in DPBS buffer (pH 7.1; Gibco, USA) for at least 1 h at RT. Samples were rinsed three times (10 min each) in 1X DPBS, then immersed in 1% osmium tetroxide combined with 1.6% potassium ferricyanide in 0.1M sodium cacodylate buffer for 1 h. Samples were rinsed three times in 0.1M sodium cacodylate buffer, then in distilled water (3 × 10 min each, RT). Tissues were dehydrated through a graded ethanol series (35%, 50%, 70%, 80%, 90%, 100%; 10 min each), treated with pure acetone (2 × 10 min), gradually infiltrated with Epon resin (EMS, Hatfield, PA) while rocking, and polymerized at 60°C for 24–48 h. Ultrathin sections of 100 nm were cut using Leica EM UC6 and UC7 microtomes and collected onto Formvar-coated 200-mesh copper grids. Alternatively, 50 nm serial sections were placed onto 1 × 2 mm slot grids covered with 0.6% Formvar film. Grids were post-stained with 2% uranyl acetate and Reynolds' lead citrate for 5 min each. Sections were imaged using a Tecnai 12 120 kV TEM (FEI, Hillsboro, OR) at the EM-Lab, University of California, Berkeley, with an UltraScan 1000 camera and Digital Micrograph 3 software (Gatan Inc., Pleasanton, CA). Collagen fiber thickness was analyzed using CurveAlign and CT-FIRE[86]; fiber alignment was assessed using structure tensor-based analysis with MATLAB code provided in the supplement.

Corneal stromal thickness

Stromal thickness was measured at the center of the cornea (the thickest region of the whole cornea) between corneal epithelial BM and cornea endothelium, from 40x cornea cross section images

RNA isolation and RNAseq library generation

Total RNA was collected at 7 days of treatment and purified using RNAaqueous and DNase reagents per the manufacturer's instructions (Ambion, Houston, TX, USA). RNA quality was assessed using the Agilent 2100 BioAnalyzer, and samples with an RNA integrity ≥6.0 were included for RNA sequencing. The synthesis of mRNA libraries was performed by Novogene Corporation Inc. according to their protocols. RNA library was formed by ployA capture (or rRNA removal), RNA fragmentation by covaris or enzyme digestion and reverse transcription of cDNA. RNA libraries were sequenced on an Illumina NovaSeq 6000 by Novogene Corporation Inc. Depths of 20–30 million 150 bp paired-end reads were generated for each sample. Quality control metrics were performed on raw sequencing reads using fastp.[87] In this step, clean data[88] (clean reads) were obtained by removing reads containing adapter and poly-N sequences and reads with low quality from raw data. At the same time, Q20, Q30 and GC content of the clean data were calculated. All the downstream analyses were based on clean data with high quality. Reference genome and gene model annotation files were downloaded from genome website browser (NCBI/UCSC/Ensembl) directly. Paired-end clean reads were aligned to the reference genome using the Spliced Transcripts Alignment to a Reference (STAR) software. DEseq2 was used to detect differential gene expression between WT, untreated Aire KO, PBS treated Aire KO and Lacripep treated Aire KO corneas based on the normalized count data. Genes were considered differentially expressed if the log2 Fold Change between samples was at least 1, with the adjusted *p*-value held to 0.05.[89] Heatmaps and Volcano plot were created using "pheatmap", and "EnhancedVolcano" R packages, respectively.

Single-nucleus (sn) RNA-sequencing and analysis

To ensure biological diversity, nuclei were initially isolated from snap frozen corneas of 5 mice per treatment group at 7 weeks of age (WT, KO, PBS). Nuclei isolation was adapted from the 10x Genomics (Sample Preparation Demonstrated protocol, Rev D). Briefly, fresh corneas were dissected, minced, snap frozen in lysis buffer (Sucrose 0.32M, $CaCl_2$ 3 mM, $Mg(Ac)_2$ 3 mM, EDTA 0.1 mM, Tris-HCL 10 mM, DTT 1 mM, Triton x100 0.1%, DEPC-treated water) and stored for further processing. Frozen samples were crushed, combined into 15 mL tube with 5 mL lysis buffer and kept on ice for 15min with vortexing every 5 min. Samples were transferred to ultracentrifuge tubes on ice (Beckman Coulter 355631), and 9 mL of sucrose solution (Sucrose 1.8M, $Mg(Ac)_2$ 3 mM, Tris-HCL 10 mM, DTT 1 mM, DEPC-treated water) was carefully added to the bottom of the tube. Samples were centrifuged at 24,400 rpm for 2.5h at 4°C, supernatant removed, and nuclei resuspended in 200 μL DEPC-based PBS. Nuclei were counted and subjected to snRNAseq using the Chromium Single Cell 3′ Reagent Version 3 Kit (10× Genomics). Sequencing was performed on an Illumina HiSeq 2500 per the 10× Genomics V3 user manual. Reads were aligned to the mouse reference genome (mm10-2020-A) using STAR and resulting bam files were processed using the Cell Ranger pipeline v6.1.2, followed by removal of ambient RNA contamination using DecontX. DecontX, is a Bayesian method, which deconvolutes the expression matrix into a matrix of native counts for each cell,and a matrix of contaminated counts, originating from other cell populations. Using Seurat v4.0 in Rstudio we filtered out low-quality cells based on UMI counts and the number of genes. The batch correction was performed with Seurat v4.0. Clustering was performed with CellFindR v2.0.0 using settings with a quality measure of ≥5 genes with FC > 1.5. Subsequent analysis was performed with Seurat v4.0. Clusters were visualized using Uniform Manifold Approximation and Projection (UMAP) dimensional reduction (RunUMAP). Markers for each cluster were identified with FindAllMarkers using default parameters. Stroma clusters were identified using the known markers Dcn and Lum and extracted from the entire cornea dataset for further analysis using Seurat and CellFindR. Regulon activity was assessed with SCENIC v1.1.2.4, SCENIC combines GENIE3[90,91] with regulatory binding motif enrichment to simultaneously cluster cells and infer regulatory networks. For cell-cell ligand-receptor interaction analysis, Seurat objects of corneal stroma data were analyzed using CellChat21 using standard parameters. Cytoscape 3.9.1 was used to visualize TF-target networks.

QUANTIFICATION AND STATISTICAL ANALYSIS

All data are expressed as mean ± SD. A minimum of three independent experimental repeats were conducted for all experiments. Statistical details including exact *n* values, what n represents, and the tests used are indicated in the figure legends. Briefly, a Student's *t* test was used for two-group comparisons; one-way ANOVA was used for multiple group comparisons with Tukey's multiple comparisons test, Dunnett T3, or Benjamini-Krieger-Yekutieli correction for false discovery rate; $p < 0.05$ was considered statistically significant. A false discovery rate of 0.05 was applied to bulk RNAseq data. A Wald test with Benjamini-Hochberg correction was used for differential gene expression analysis.